Supporting information

Table of contents

1. General experimental methods

All the solvents and chemicals were of reagent grade and were used without purification. NMR spectra were recorded on a Bruker Avance ll 500. ^{1}H spectra were recorded at 500 MHz. ^{13}C NMR spectra were recorded at 125 MHz. 2D NMR spectra were recorded to complete signal assignments. ^{1}H NMR spectra were referenced to residual protiated solvents (1.96 ppm (δ_{Me}) for CD_3CN, 7.26 ppm (δ_H) for $CDCl_3$). Chloroform ($CHCl_3$ or $CDCl_3$) saturated with water was prepared by vigorous shaking of two equivalent volumes of solvents and collected after phase separation in a separatory funnel (operation repeated three times). UV-vis spectra were collected with a JASCO V770 at room temperature. IR spectra were obtained with a Perkin-Elmer Spectrum on FTIR spectrometer equipped with a MIRacleTM single reflection horizontal ATR unit (germanium crystal). Optical rotations (α_D) were measured in $CHCl_3$ saturated with H_2O on a Perkin Elmer polarimeter (model 341) at 20 °C with a sample cell of 1 dm. Circular dichroism spectra were collected on a JASCO J-815 spectropolarimeter at room temperature in solution ($CHCl_3$ saturated with H_2O). MS-ESI analyses were performed on a Thermofinnigan LCQ Advantage spectrometer and HRMS analyses were performed on Thermoscientifc exactive using methanol or acetonitrile as solvents.

EPR spectra were recorded at T = 100 K or at room temperature using a Bruker Elexsys E500 EPR spectrometer (Bruker, Wissembourg, France), operating at X-band (9.8 GHz) and equipped with a SHQ high-sensitivity cavity and a Variable Temperature Unit (Bruker ER4141VTM) for low temperature experiments.

Typical settings used were: microwave power, 10 mW; modulation frequency, 100 kHz; modulation amplitude, 0.6 mT; receiver gain, 42 dB; time constant, 5.12 ms; conversion time, 20.48 ms; datapoints, 2048; sweep width, 160 mT; sweep time, 41.94 s. Each spectrum is the sum of 4 spectra.

The magnetic field at the sample position was corrected using a Bruker weak pitch standard sample for which the g-value is accurately known. The g-values were determined from the corrected magnetic field at the centre of the EPR line and the microwave frequency read from the frequency meter.

Data acquisition and processing were performed using Bruker Xepr software. The simulated spectra were calculated with the EasySpin toolbox working on MatLab platform.[1]

Encapsulation of the metal complexes restored the anisotropy of the EPR spectra usually observed in frozen solutions. Therefore, we assumed that the rotational motion could be neglected for spectral simulations and the EasySpin function pepper designed for simulations of solid-state continuous wave EPR spectra was used.

Safety Note. Caution! Although we have not encountered any problems, it is noted that perchlorate salts of metal complexes with organic ligands and azide species are potentially explosive and must be handled only in small quantities with appropriate precautions.

2. Synthesis and characterisation

$Zn(H_2O)_6(CSA)_2$,[2] $Cu(H_2O)_6(CSA)_2$,[3] resorcinarene **1**,[4] TMPA ligand **2**,[5] **[Cu(TMPA)Cl]PF_6**,[6] **[Cu(TMPA)H_2O]$(ClO_4)_2$** [7] and **[Cu(TMPA)Cl]BAr^F** [8] were synthesised and characterised following methods previously described in the literature.

[Cu(TMPA)N_3]ClO_4.

This complex was synthesised according to the protocol reported by Wada et al.[9]

In a 10 ml round bottom flask, 2 ml of MeOH containing 97.5 mg (0.336 mmol) of TMPA and 124.4 mg (0.336 mmol) of $Cu(H_2O)_6(ClO_4)_2$ were stirred for 15 min at room temperature. Then, 22.9 mg of NaN_3 (0.353 mmol) were dissolved in 1 ml of MeOH and added to the solution. The resulting solution was sonicated and stirred. After 1 hour, the resulted green precipitate was filtered and washed with 1 ml of cold MeOH. A second washing of the filtrate was done by adding 3 ml of water. After drying, the product was obtained as a green precipitate in 70 % yield (m=117 mg).

UV-vis ($CHCl_3$ sat H_2O): λ/nm (ε/M^{-1}. cm^{-1}) 424 (2620), 671 (262), 881 (231)

HRMS-ESI+ (m/z) calcd. for $C_{18}H_{18}CuN_7$ ($[M]^+$) 395.0902, found 395.0903

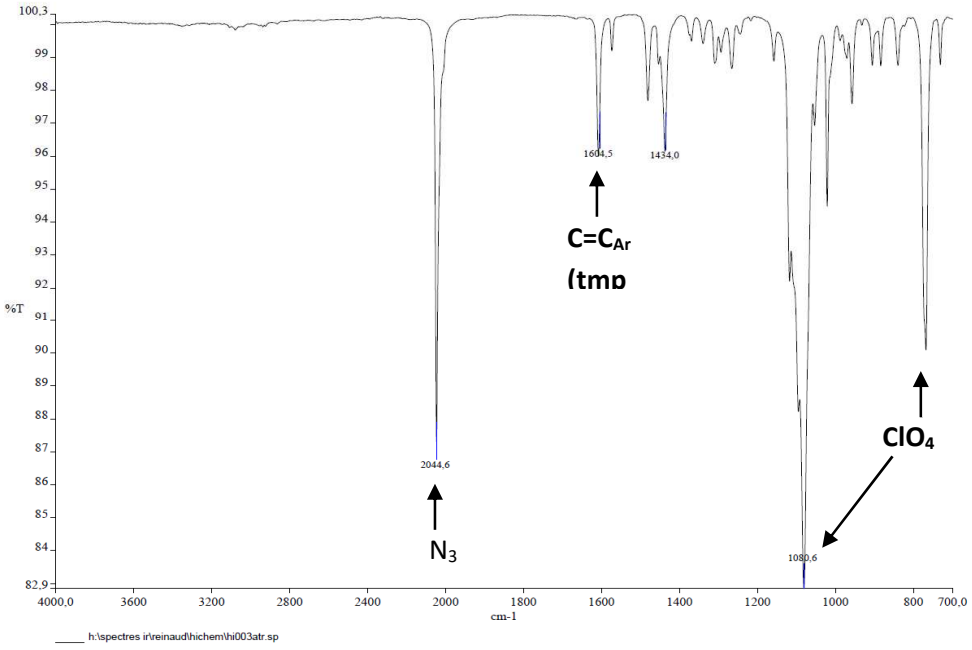

Figure S1. FTIR spectrum (ATR) of **[Cu(TMPA)N_3]ClO_4**

[Cu(TMPA)N_3]BAr^F

This complex was prepared via anion metathesis according to an adapted procedure (Copper TMPA complex was used instead of the Zinc complex) from the original method mentioned in the literature.[10]

In a 25 ml round bottom flask, 128.8 mg (0,145 mmol) of $NaBAr^F$ and 71.8 mg (0,145 mmol) of **$[Cu(TMPA)N_3]ClO_4$** were dissolved in 13.5 ml of diethyl ether. The mixture was sonicated and stirred for 4 h at room temperature. After that, the precipitate ($NaClO_4$) was removed by filtration and the solvent was evaporated. A green precipitate was recovered in 96% yield (175 mg). The product was characterised by HRMS-ESI+, UV-vis and IR-ATR where we observed the disappearance of the ClO_4 characteristic bands and the appearance of three new bands that correspond to BAr^F the bands.

UV-vis ($CHCl_3$ sat H_2O): λ/nm (ε/M^{-1}. cm^{-1}) 436 (2913), 678 (316), 889 (250)

MS-ESI+ (m/z) calcd. for $C_{18}H_{18}CuN_7$ ($[M]^+$) 395.0902, found 395.0903

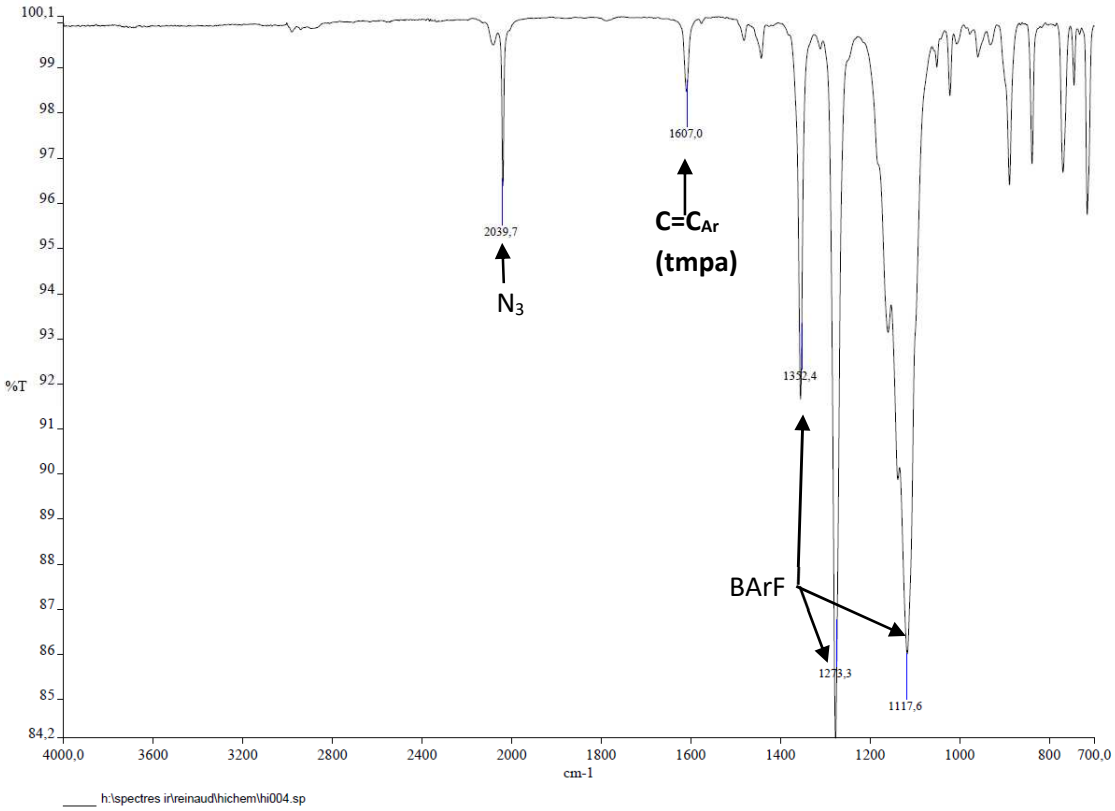

Figure S2. FTIR spectrum (ATR) of **$[Cu(TMPA)N_3]BAr^F$.**

[Zn(TMPA)Cl][(+)CSA]

To a solution of TMPA (89.5 mg, 0.31 mmol) in 5 mL of methanol was added $Zn(H_2O)_6[(+)CSA]_2$ (187.3 mg, 0.31 mmol). After 10 minutes of stirring at rt, NaCl was added (19.5 mg, 0.32 mmol). The mixture was stirred for 2h at rt. After evaporation of the methanol, 10ml of DCM was added, the mixture was put 30 minutes in a freezer and the precipitate was filtered. The filtrate was evaporated and dried on P_2O_5 under vacuum. The product was obtained as a slight yellow powder. Yield = 92 % (176.8 mg). The integrations of the peaks corresponding to the TMPA ligand and the CSA anion confirmed the 1:1 ratio between the Zn(TMPA)Cl cation and the CSA anion.

^{1}H NMR ($CDCl_3$ sat H_2O, 298 K, 500 MHz): 0.86 (s, 3H), 1.14 (s, 3H), 1.38 (m, 1H), 1.86 (m, 1H), 1.90 (d, J = 20 Hz, 2.04 (m, 2H), 2.35 (dt, J = 18.5 Hz, J = 4 Hz, 1H), 2.83 (m, 1H), 2.90 (d, J = 14.5Hz, 1H), 3.42 (d, J=14.5Hz, 1H), 4.54 (d, J = 16.5 Hz, 3H), 4.60 (d, J = 16.5 Hz, 3H), 7.52 (t, J = 5.0 Hz, 3H), 7.73 (d,

J=7.5Hz,3H), 7.96 (t, J=7.5Hz, 3H), 9.07 (d, J = 5.0 Hz, 3H). ^{13}C NMR ($CDCl_3$ sat H_2O, 298 K, 125 MHz): 20.1, 20.3, 24.8, 27.4, 42.8, 43.3, 47.4, 48.3, 56.8, 58.8, 125.0, 125.4, 141.4, 149.2, 156, 217.7.

$[\alpha]_D^{20}$ = + 14.5 +/- 2.9 (2.08 mg in 2 mL $CHCl_3$ sat H_2O, 298 K)

MS-ESI+ (m/z) calcd. for $C_{18}H_{18}ZnClN_4$ ($[M]^+$) 389.0506, found 389.0502

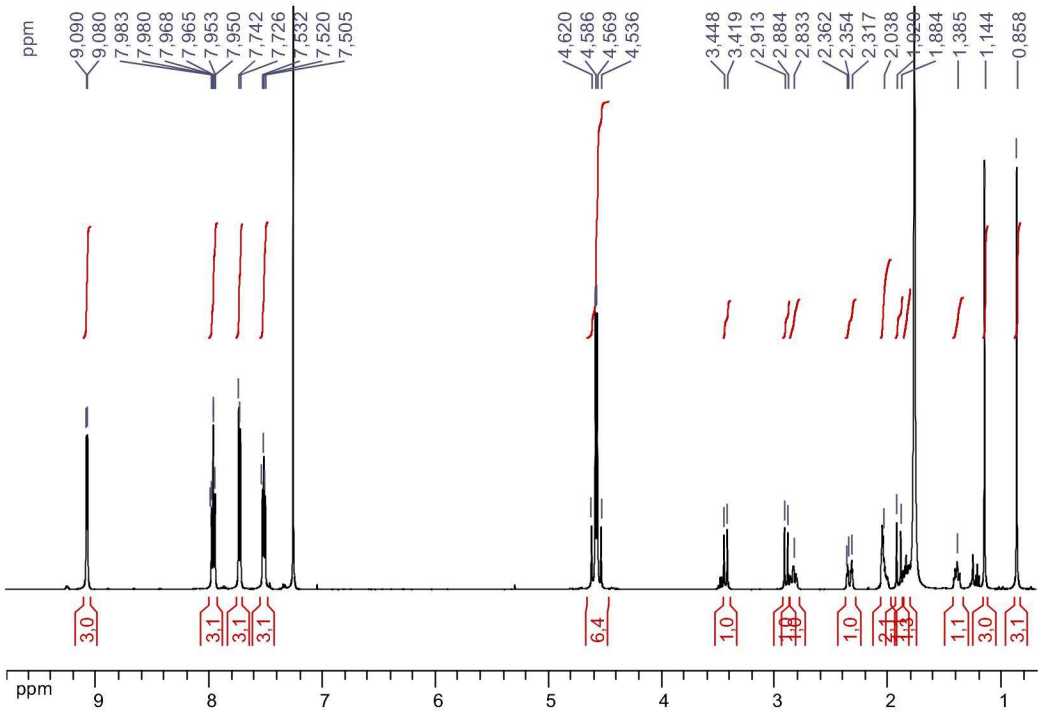

Figure S3. ^{1}H NMR spectrum ($CDCl_3$ sat. H_2O, 293 K) of **[Zn(TMPA)Cl][(+)CSA]**.

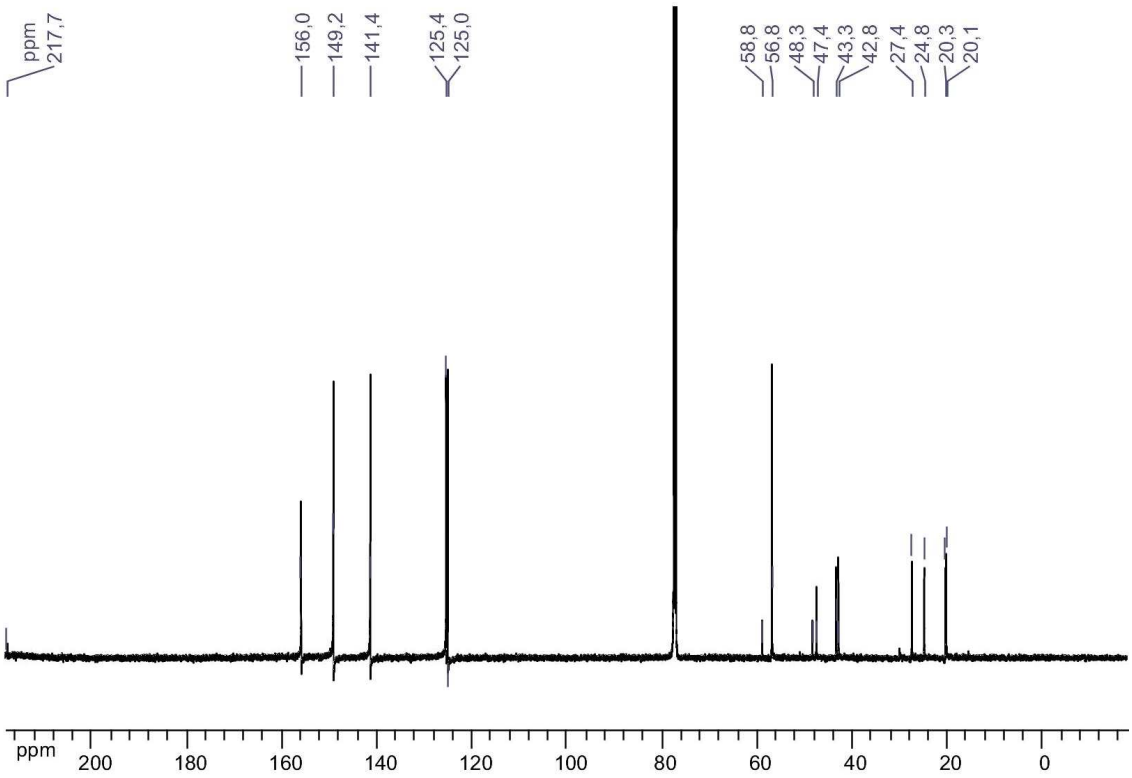

Figure S4. ^{13}C NMR spectrum ($CDCl_3$ sat. H_2O, 293 K) of **[Zn(TMPA)Cl][(+)CSA]**.

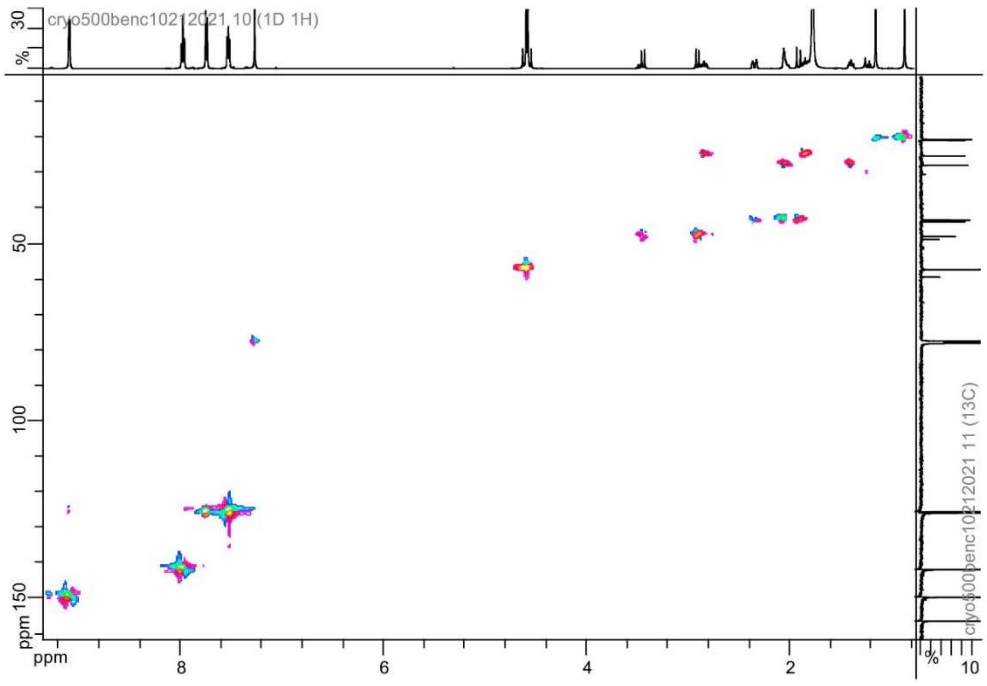

Figure S5. HSQC NMR spectrum ($CDCl_3$ sat. H_2O, 293 K) of **[Zn(TMPA)Cl][(+)CSA]**.

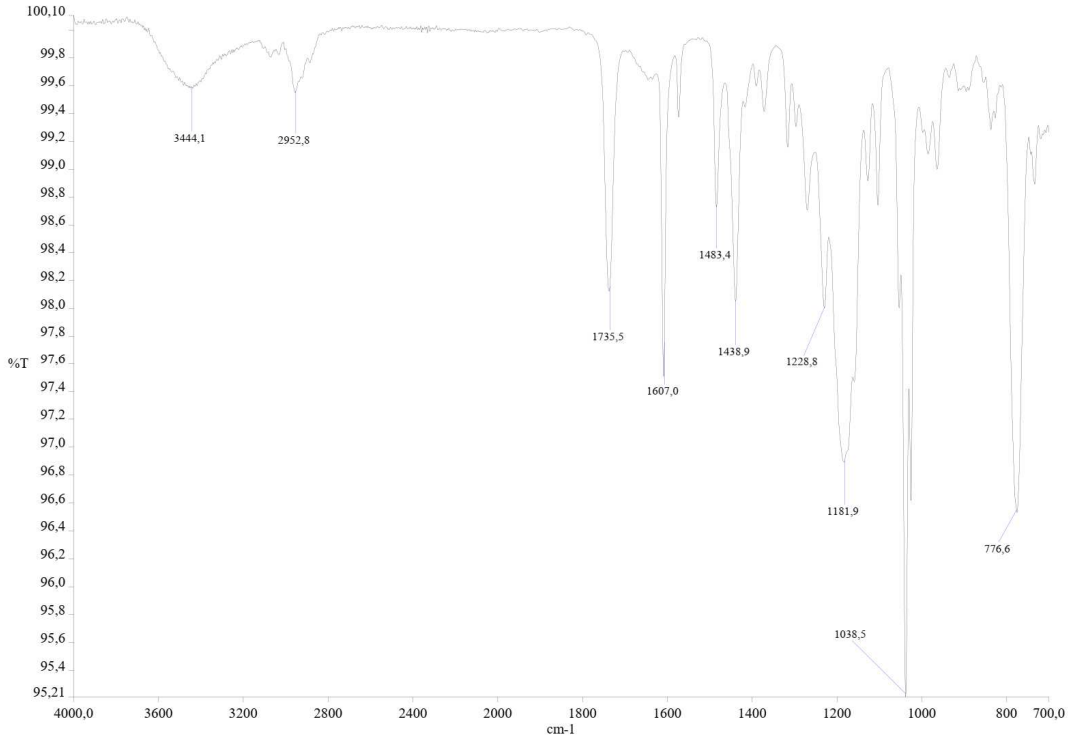

Figure S6. FTIR (ATR) of **[Zn(TMPA)Cl][(+)CSA]**.

The copper complexes with **CSA** counter ions were prepared following the same procedure.

[Cu(TMPA)Cl][(+)CSA]

To a solution of TMPA (60.7 mg, 0.21 mmol) in 5 mL of methanol was added $Cu(H_2O)_6[(+)CSA]_2$ (113.8 mg, 0.21 mmol). After 10 minutes of stirring at rt, NaCl was added (12.3 mg, 0.21 mmol). The mixture was stirred for 2h at rt. After evaporation of the methanol, 10ml of DCM was added, the mixture was put 30 minutes in a freezer and the precipitate was filtered. The filtrate was evaporated and dried on P_2O_5 under vacuum. The product was obtained as a green powder. Yield = 93 % (121 mg).

UV-vis ($CHCl_3$ sat H_2O): λ/nm (ε/$M^{-1}.cm^{-1}$) 725 (65), 946 (170)

$[\alpha]_D^{20}$ = + 19.0 +/- 3.8 (2.10 mg in 2 mL $CHCl_3$ sat H_2O, 298 K)

MS-ESI+ (m/z) calcd. for $C_{18}H_{18}CuClN_4$ ($[M]^+$) 388.0510, found 388.0508

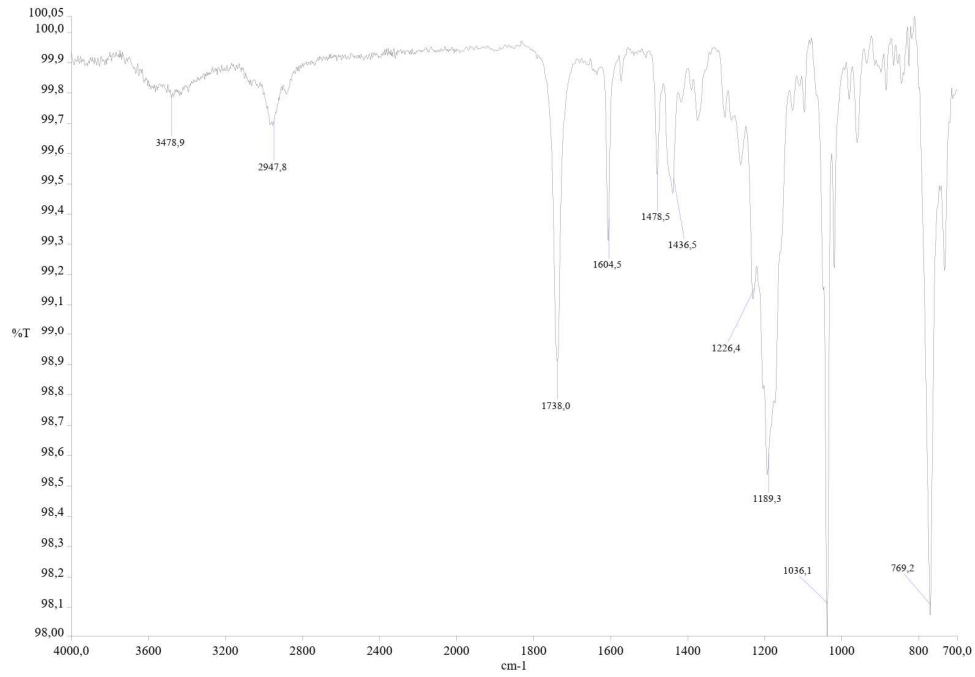

Figure S7. FTIR (ATR) of **[Cu(TMPA)Cl][(+)CSA]**.

[Cu(TMPA)Cl][(-)CSA]

Same procedure as for **[Cu(TMPA)Cl][(+)CSA]** with 91 mg of TMPA and 176 mg of $Cu(H_2O)_6[(-)CSA]_2$ to obtain 175.5 mg of product (90% yield).

$[\alpha]_D^{20}$ = - 12.0 +/- 2.4 (2.07 mg in 2 mL $CHCl_3$ sat H_2O, 298 K)

UV-vis ($CHCl_3$ sat H_2O): λ/nm (ε/M^{-1}. cm^{-1}) 725 (65), 946 (170)

MS-ESI+ (m/z) calcd. for $C_{18}H_{18}CuClN_4$ ($[M]^+$) 388.0510, found 388.0509

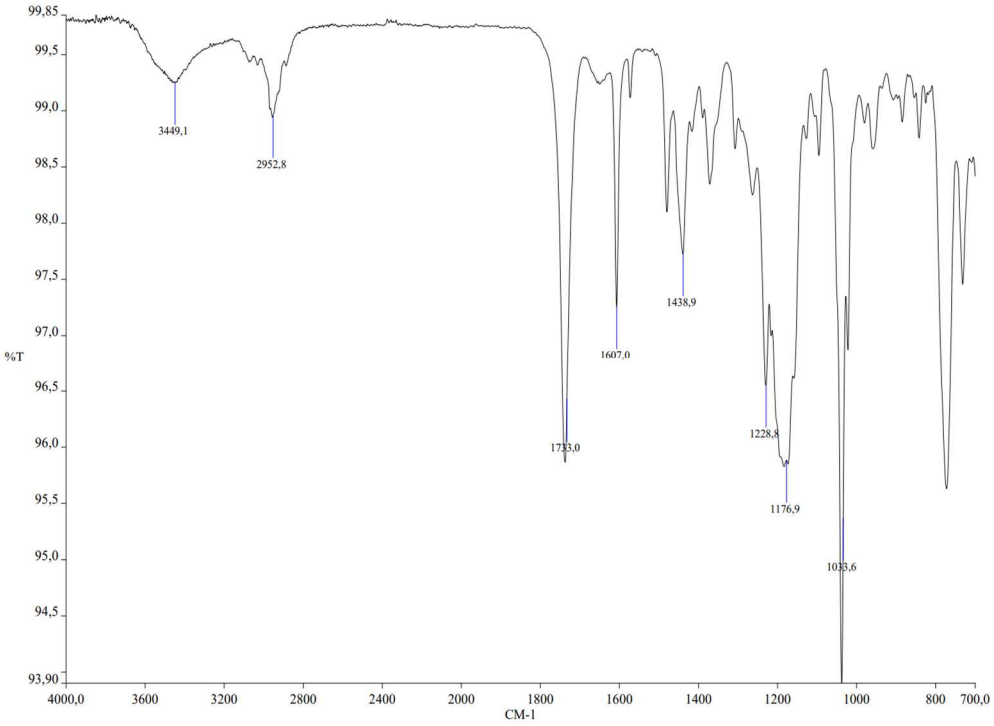

Figure S8. FTIR spectrum (ATR) of **[Cu(TMPA)Cl][(-)CSA]**.

3- Characterisation of the encapsulation by UV-vis and EPR spectroscopies

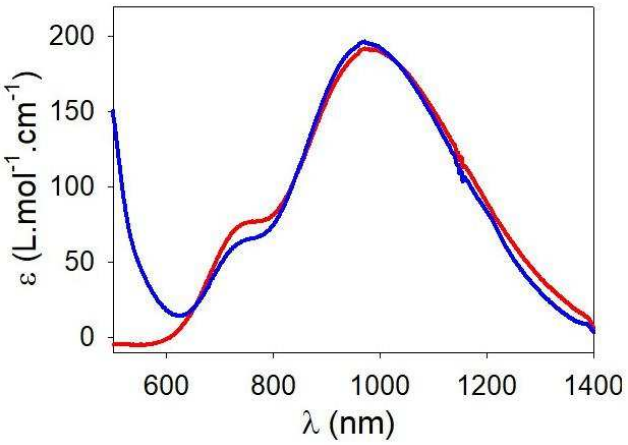

Figure S9. UV-vis spectra of **[TMPACuCl](BAr^F)** (red) and **[TMPACuCl@1_6](BAr^F)** (blue) ($CHCl_3$, 298 K).

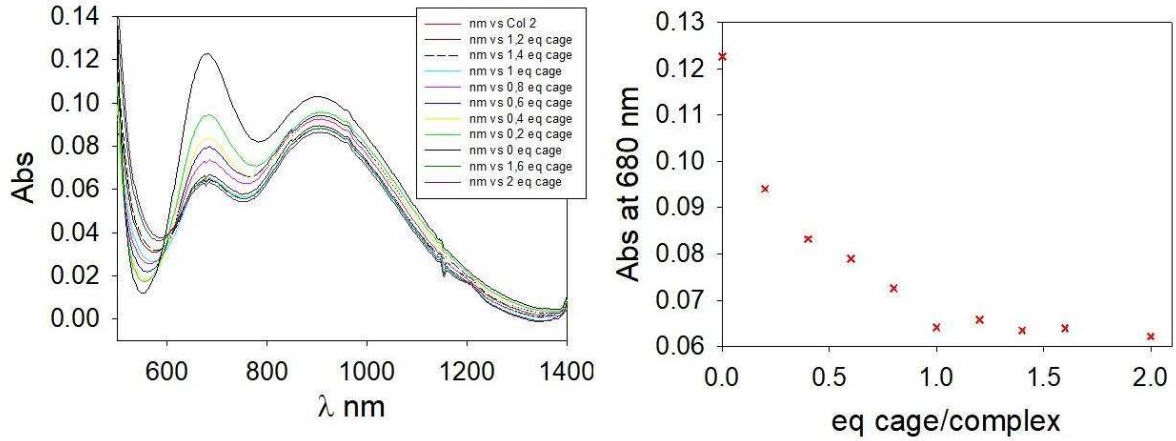

Figure S10. Left: titration experiment monitored by UV-vis spectroscopy of **[TMPACuN$_3$](BAr^F)** and **1_6** ($CHCl_3$, 298 K, 500 µM). Right: binding isotherm following the variation of the absorbance at 680 nm.

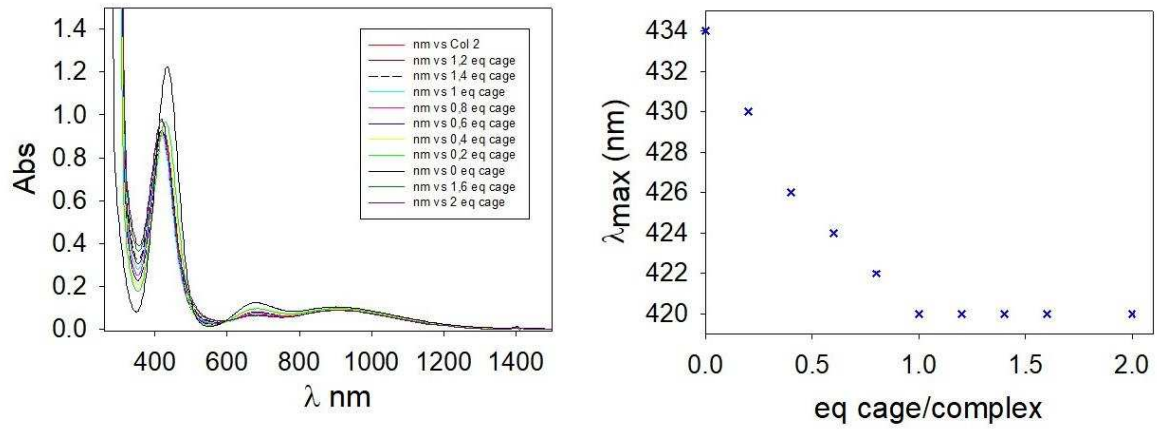

Figure S11. Left: titration experiment monitored by UV-vis spectroscopy of **[TMPACuN$_3$](BAr^F)** and **1_6** ($CHCl_3$, 298 K, 500 µM). Right: binding isotherm following the variation of the maximum of absorbance of the LMCT band.

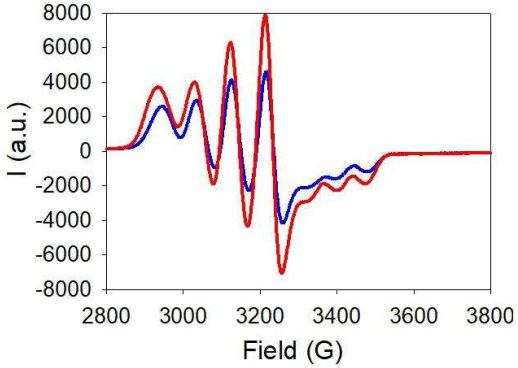

Figure S12. EPR spectra of **[TMPACuN$_3$](BAr^F)** (blue) and a 1:1 mixture of **[TMPACuN$_3$](BAr^F)** and **1$_6$** (red) ($CHCl_3$, 115 K, 3 mM).

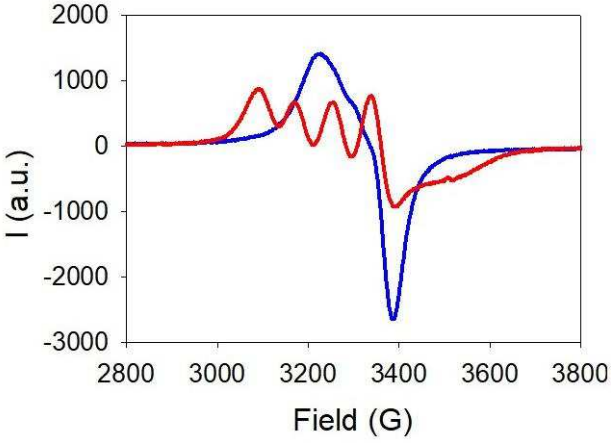

Figure S13. EPR spectra of **[TMPACuCl](BAr^F)** (blue) and a 1:1 mixture of **[TMPACuCl](BAr^F)** and **1$_6$** (red) ($CHCl_3$, 298 K, 3 mM).

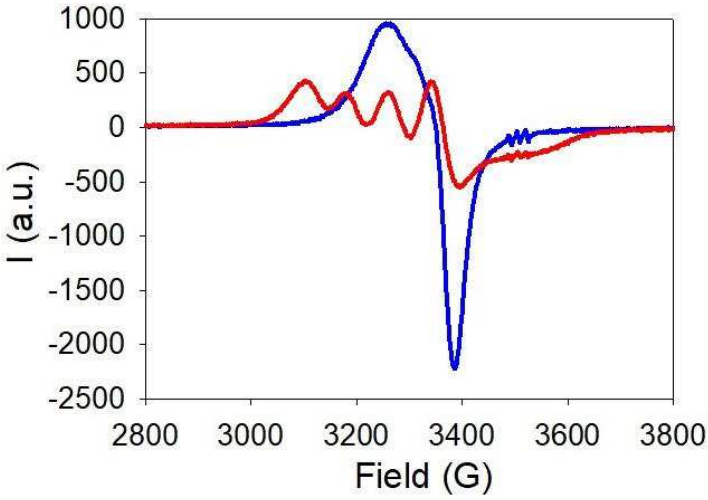

Figure S14. EPR spectra of **[TMPACuN$_3$](ClO$_4$)** (blue) and a 1:1 mixture of **[TMPACuN$_3$](ClO$_4$)** and **1$_6$** (red) ($CHCl_3$, 298 K, 2 mM).

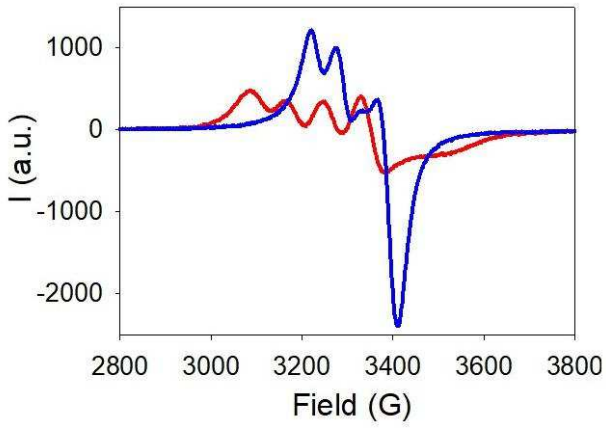

Figure S15. EPR spectra of **[TMPACuCl](PF$_6$)** (blue) and a 1:1 mixture of **[TMPACuCl](PF$_6$)** and **1$_6$** (red) ($CHCl_3$, 298 K, 2 mM).

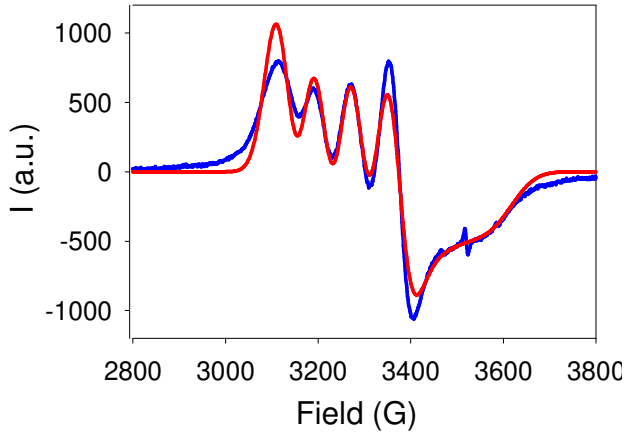

Figure S16. EPR spectrum of a 1:1 mixture of **[TMPACuN$_3$](BAr^F)** and **1$_6$** (blue) ($CHCl_3$, 298 K) and the simulated spectrum (red).

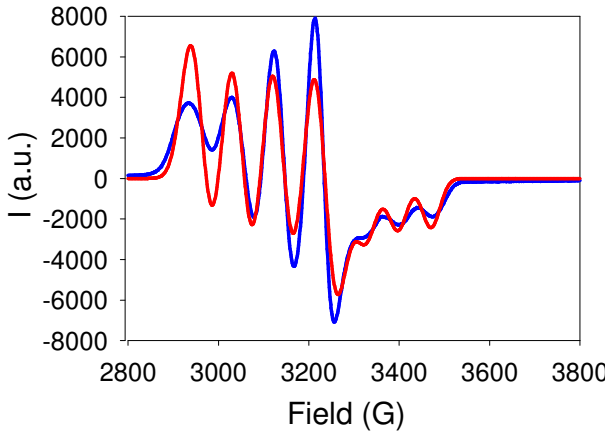

Figure S17. EPR spectrum of a 1:1 mixture of **[TMPACuN$_3$](BAr^F)** and **1$_6$** (blue) ($CHCl_3$, 115 K) and the simulated spectrum (red).

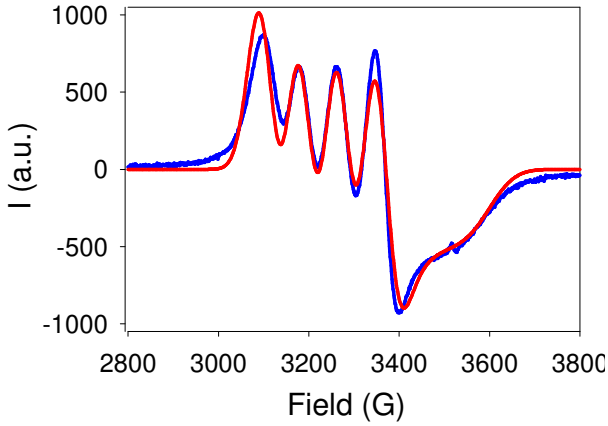

Figure S18. EPR spectrum of a 1:1 mixture of **[TMPACuCl](BAr^F)** and **1$_6$** (blue) ($CHCl_3$, 298 K) and the simulated spectrum (red).

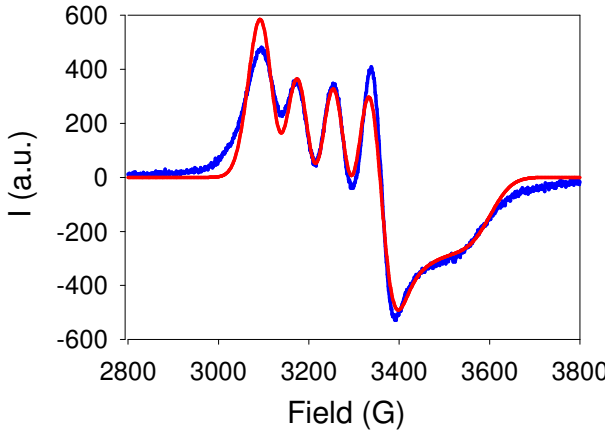

Figure S19. EPR spectrum of a 1:1 mixture of **[TMPACuCl](PF$_6$)** and **1$_6$** (blue) ($CHCl_3$, 298 K) and the simulated spectrum (red).

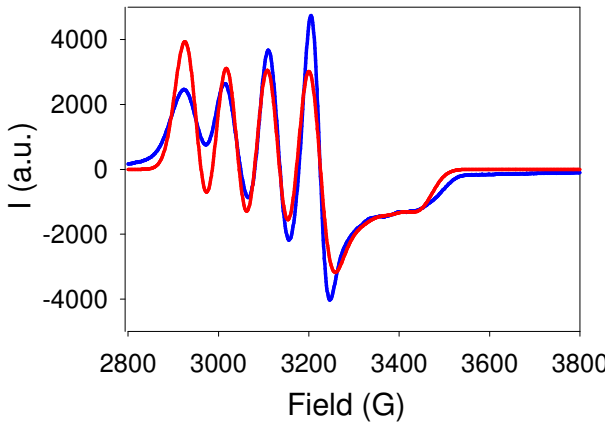

Figure S20. EPR spectrum of a 1:1 mixture of **[TMPACuCl](PF$_6$)** and **1$_6$** (blue) ($CHCl_3$, 115 K) and the simulated spectrum (red).

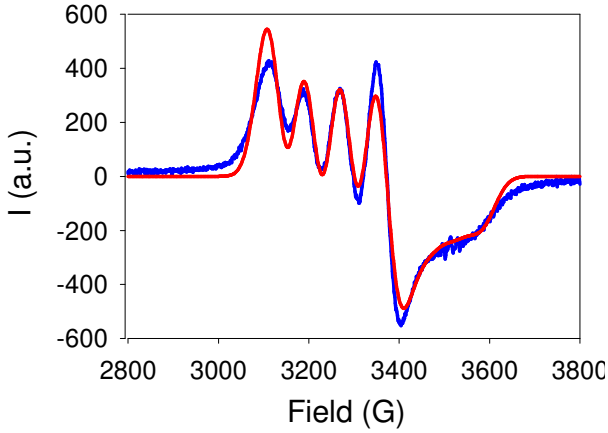

Figure S21. EPR spectrum of a 1:1 mixture of **[TMPACuN$_3$](ClO$_4$)** and **1$_6$** (blue) ($CHCl_3$, 298 K) and the simulated spectrum (red).

Complex in **1$_6$**	T (K)	**$g_\perp$**	**$g_\parallel$**	**$A_\perp$**		**$A_\parallel$**	
				MHz	**G**	**MHz**	**G**
[TMPACuN$_3$](BAr^F)	298	2.173	2.003	235	83.8	-	
[TMPACuN$_3$](BAr^F)	115	2.186	2.006	271	96.7	193	68.9
[TMPACuN$_3$](ClO$_4$)	298	2.175	2.013	235	83.8	-	
[TMPACuCl](PF$_6$)	298	2.183	2.012	236	84.2	-	
[TMPACuCl](PF$_6$)	115	2.194	2.009	272	97.1	-	
[TMPACuCl](BAr^F)	298	2.181	2.015	252	90.0	-	
[TMPACu(H$_2$O)](ClO$_4$)$_2$	298	2.196	2.015	282	101	-	

Table S1. EPR Spectroscopy parameters of the encapsulated complexes: g-values and hyperfine coupling constants A (MHz left column and G right column) obtained by simulation.

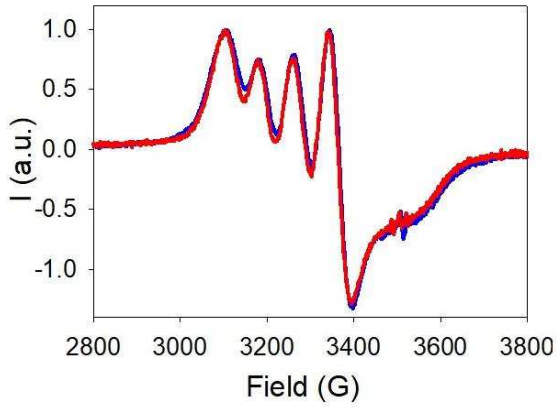

Figure S22. EPR normalised spectra of a 1:1 mixture of $\mathbf{1_6}$ and **[TMPACuN$_3$](BAr^F)** (blue) or **[TMPACuN$_3$](ClO$_4$)** (red) ($CHCl_3$, 298 K).

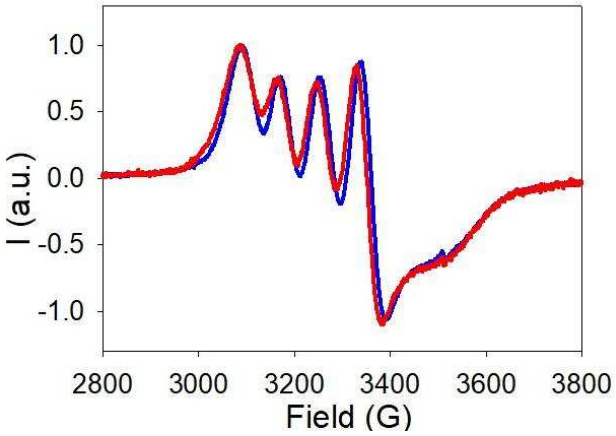

Figure S23. EPR normalised spectra of a 1:1 mixture of $\mathbf{1_6}$ and **[TMPACuCl](BAr^F)** (blue) or **[TMPACuCl](PF$_6$)** (red) ($CHCl_3$, 298 K).

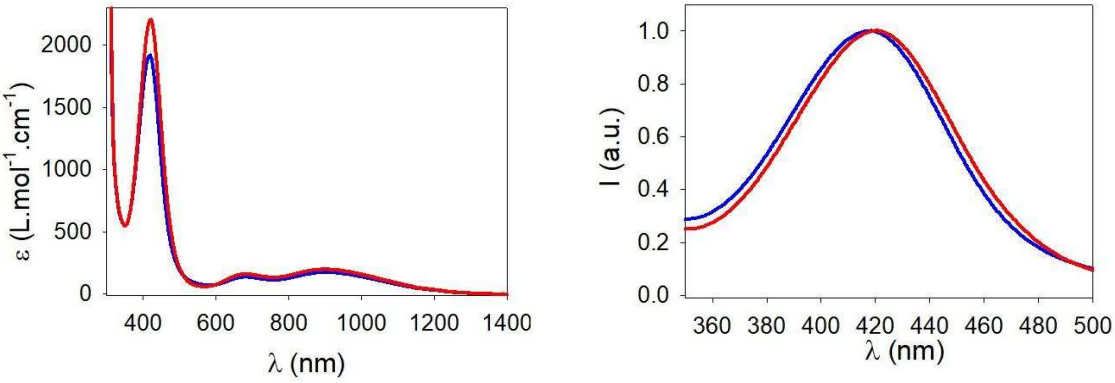

Figure S24. Left: UV-vis spectra of a 1:1 mixture of $\mathbf{1_6}$ and **[TMPACuN$_3$](BAr^F)** (red) or **[TMPACuN$_3$](ClO$_4$)** (blue) ($CHCl_3$, 298 K). Right: Normalised UV-vis spectra in the region of the LMCT band for a 1:1 mixture of $\mathbf{1_6}$ and **[TMPACuN$_3$](BAr^F)** (red) or **[TMPACuN$_3$](ClO$_4$)** (blue).

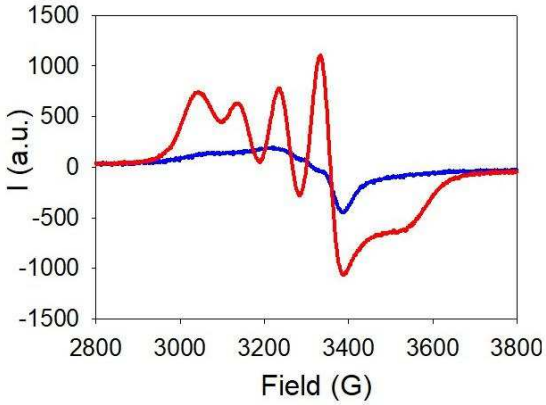

Figure S25. EPR spectra of **[TMPACu(H$_2$O)](ClO$_4$)$_2$** (blue) and a 1:1 mixture of **[TMPACu(H$_2$O)](ClO$_4$)$_2$** and **1$_6$** (red) ($CHCl_3$, 298 K, 2 mM).

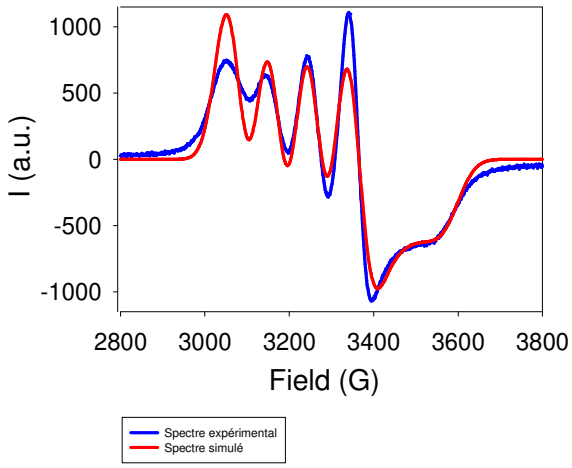

Figure S26. EPR spectrum of a 1:1 mixture of **[TMPACu(H$_2$O)](ClO$_4$)$_2$** and **1$_6$** (blue) ($CHCl_3$, 298 K) and the simulated spectrum (red).

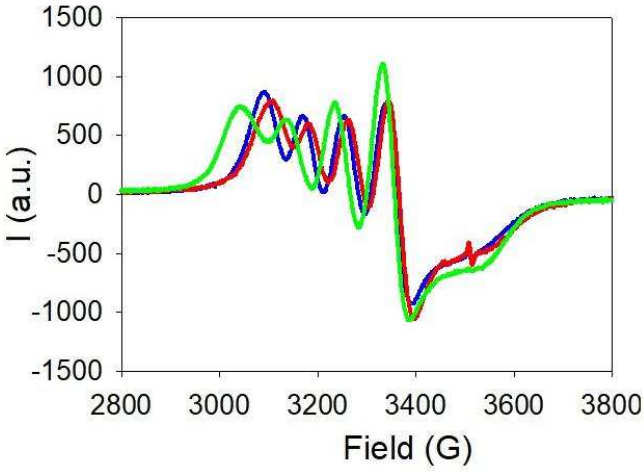

Figure S27. EPR spectra of a 1:1 mixture of **1$_6$** and **[TMPACuCl](BAr^F)** (blue) or **[TMPACuN$_3$](BAr^F)** (red) and **[TMPACu(H$_2$O)](ClO$_4$)$_2$** (green) ($CHCl_3$, 298 K, 2 mM).

4- Characterisation of the encapsulation of chiral complexes

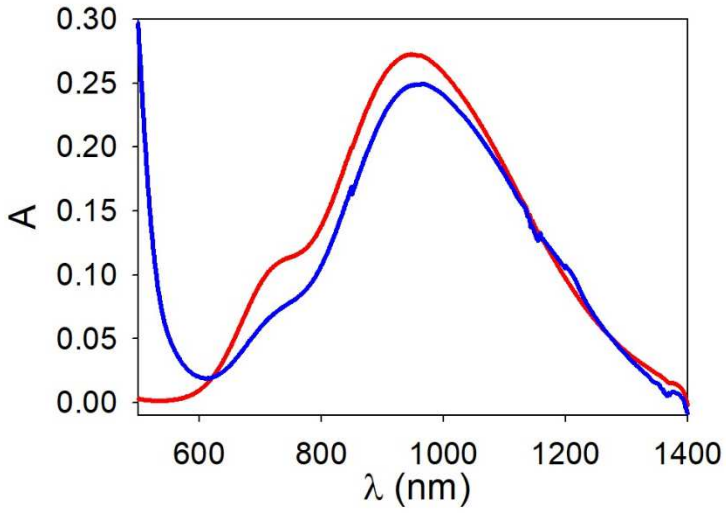

Figure S28. UV-vis spectra ($CHCl_3$ sat. H_2O, 298 K, 1.5 mM) of **[Cu(TMPA)Cl][(+)CSA]** (red) and with one equivalent of cage $\mathbf{1_6}$ (blue).

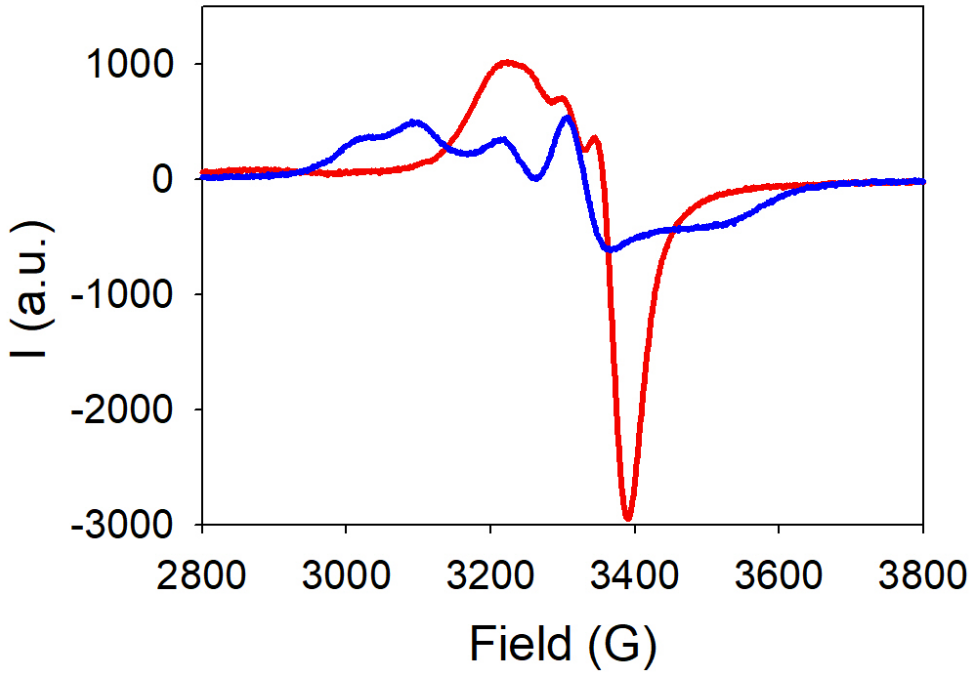

Figure S29. EPR spectra ($CHCl_3$ sat. H_2O, 298 K, 2 mM) of **[Cu(TMPA)Cl][(+)CSA]** (red) and with one equivalent of cage $\mathbf{1_6}$ (blue).

	(+)CSA	(-)CSA
[Cu(TMPA)Cl]	+ 19 ± 3.8	-11,6 ±2.3
[Cu(TMPA)Cl] with 1.2 eq of 1_6	- 47 ± 9.4	+ 42 ± 8.4

Table S2. Values of the specific rotation measured in $CHCl_3$ sat. H_2O at 298 K. The reported values are the mean values of at least 3 measurements.

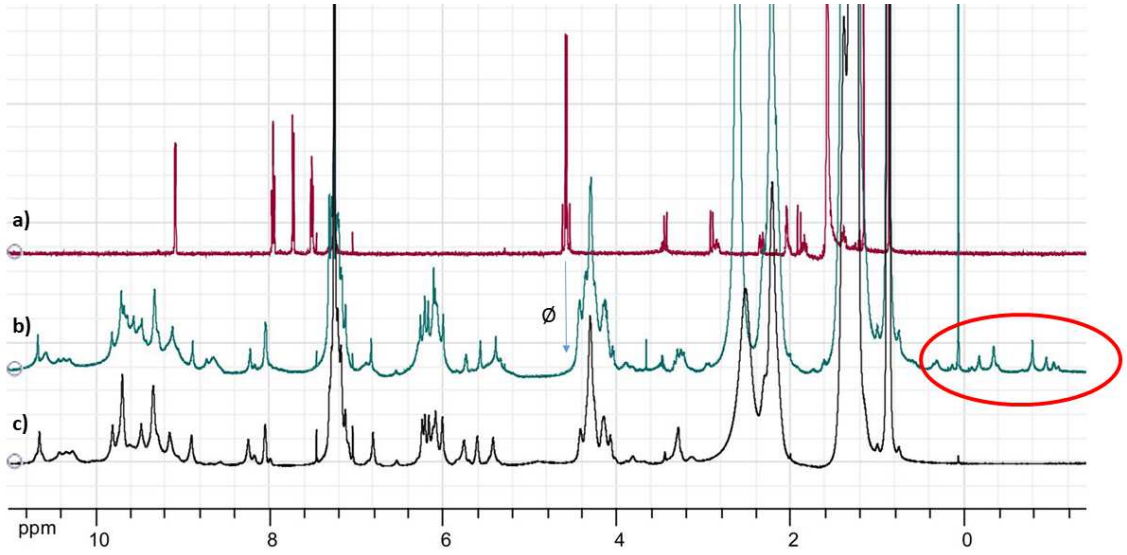

Figure S30. ^1H NMR spectrum ($CDCl_3$ sat. H_2O, 293 K) of a) **[Zn(TMPA)Cl][(+)CSA]**, b) **[Zn(TMPA)Cl][(+)CSA]** and 1 eq of $\mathbf{1_6}$ and c) **[Zn(TMPA)Cl][$(ZnCl_4)_{1/2}$]** and 1 eq of $\mathbf{1_6}$.

5- Kinetic studies

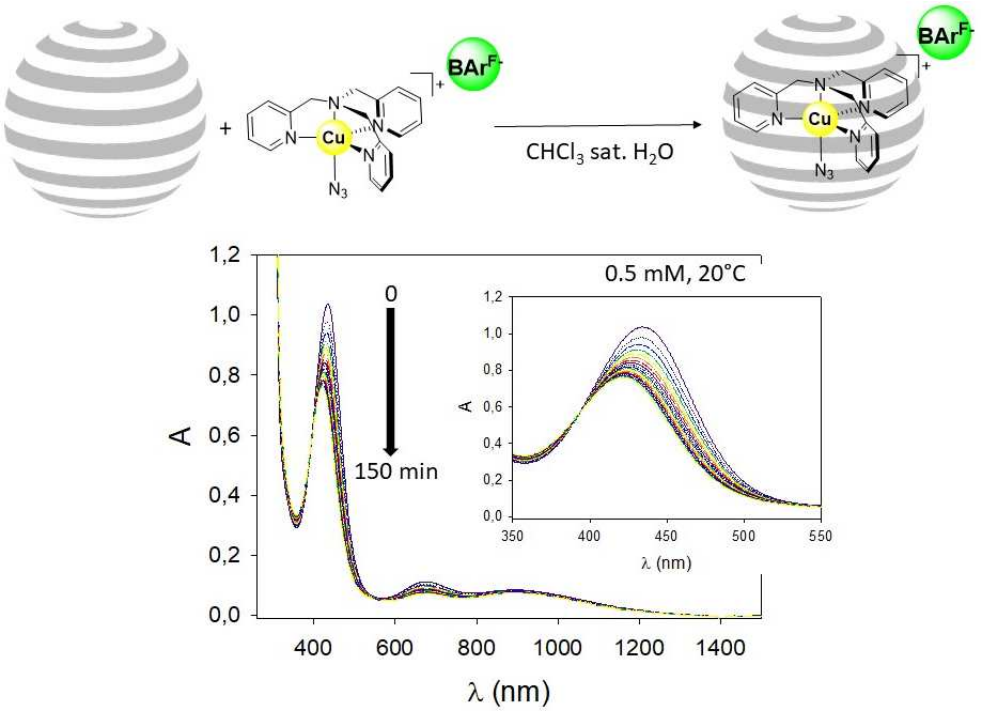

Figure S31. Kinetic experiment for the encapsulation of **[TMPACuN$_3$](BAr^F)** in **1$_6$** monitored by UV-vis spectroscopy (CHCl$_3$, 293 K, 0.5 mM in both species). Data are collected every 4 min during 150 min.

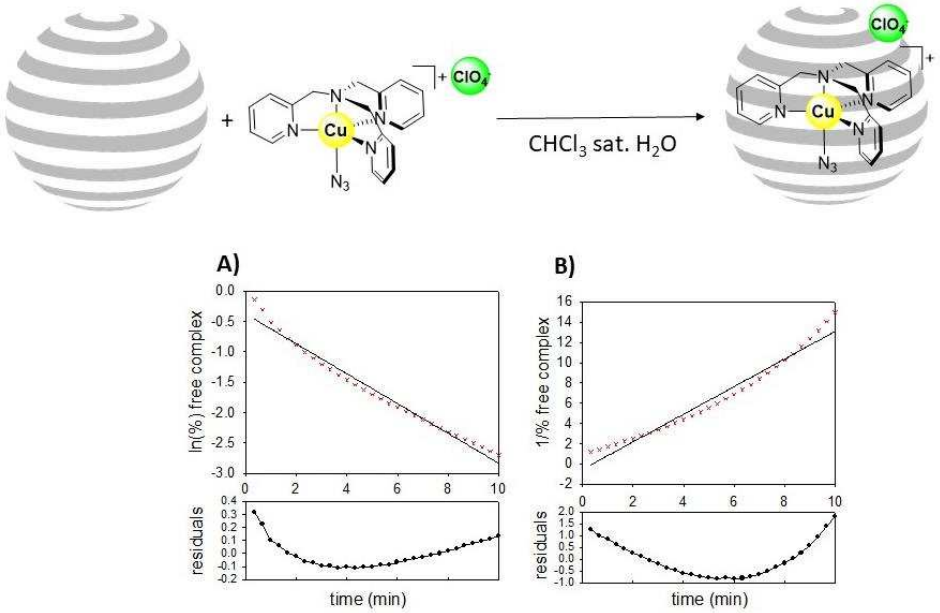

Figure S32. Fitting of the free complex decay and residuals for the determination of the overall order of the encapsulation of **[TMPACuN$_3$](ClO$_4$)** in **1$_6$** with a first-order (A) or second-order (B) hypothesis (CHCl$_3$, 293 K, 0.5 mM in both species).

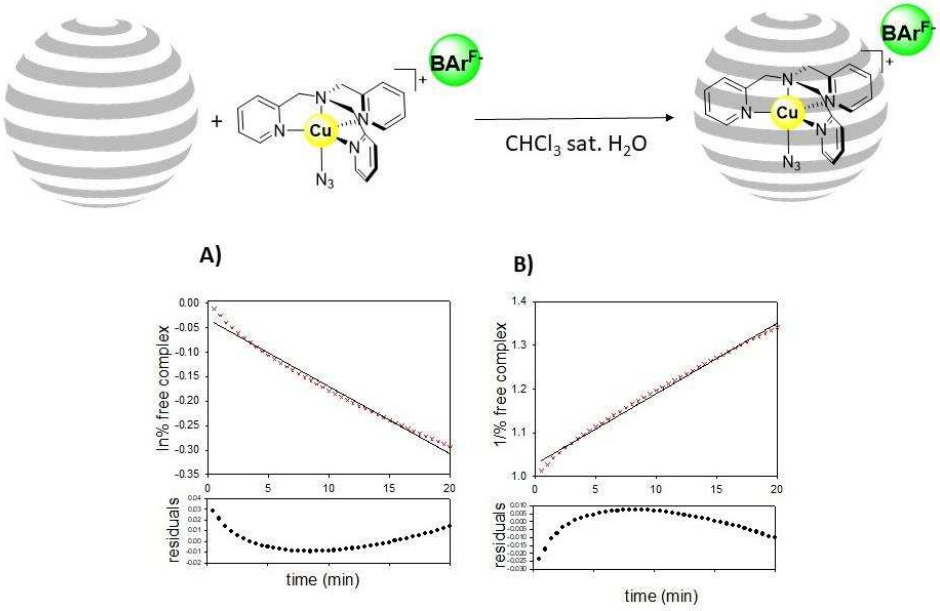

Figure S33. Fitting of the free complex decay and residuals for the determination of the overall order of the encapsulation of **[TMPACuN$_3$](BAr^F)** in **1$_6$** with a first-order (A) or second-order (B) hypothesis ($CHCl_3$, 293 K, 0.5 mM in both species).

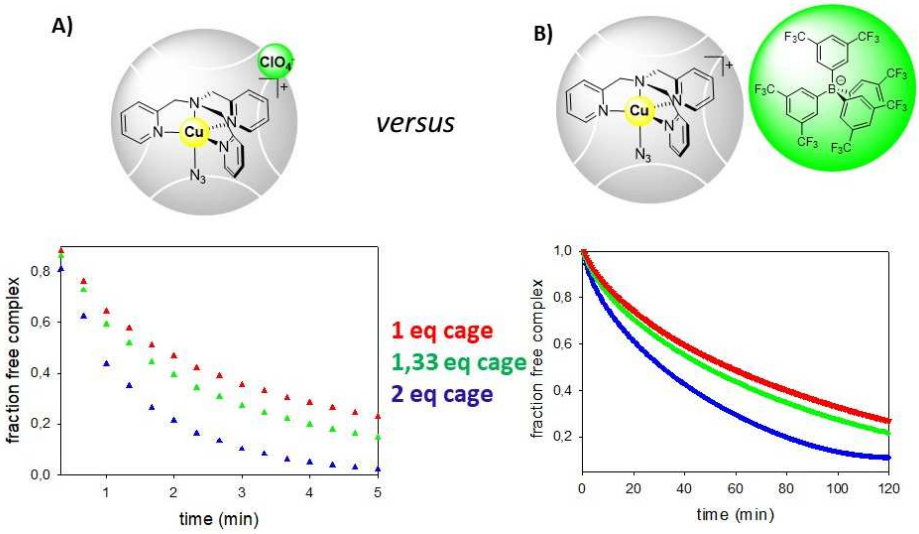

Figure S34. Fraction of free **[TMPACuN$_3$](X)** as a function of time during its encapsulation in **1$_6$** with **X** = **ClO$_4$** (A) and **X** = **BAr^F** (B) ($CHCl_3$, 293 K, [**[TMPACuN$_3$](X)**]$_0$ = 0.5 mM and variable [**1$_6$**]$_0$).

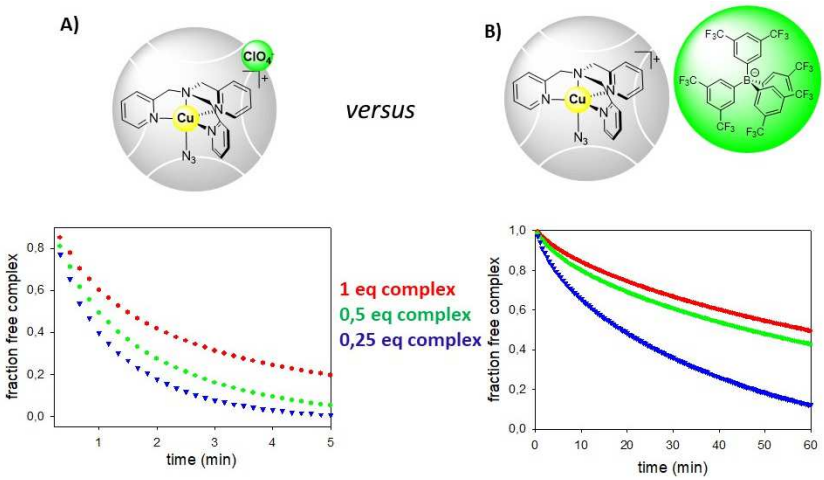

Figure S35. Fraction of free **[TMPACuN$_3$](X)** as a function of time during its encapsulation in **1$_6$** with **X** = **ClO$_4$** (A) and **X** = **BAr^F** (B) ($CHCl_3$, 293 K, [**1$_6$**]$_0$ = 0.75 mM and variable [**[TMPACuN$_3$](X)**]$_0$).

6- Molecular Dyamics simulations.

Simulation parameters

The initial ligand-cage system is based on a previous docking calculation for the system $CuTMPAN_3$ inserted in a resorcinarene cage $\mathbf{1}_6^1$.[10]The cage contains eight structuring water molecules organised to stabilise the resorcinarene cage through hydrogen bonds. The coordinates of the BAr^{F-} and ClO_4^- ions were obtained from the crystallographic structures YEMZUL01[11] and $CuTMPAN_3$.cif,[9] respectively. Hydrogen atom locations were optimised at the QM B3LYP-631G* level of theory using the program Gaussian.[12] The program Avogadro was used to add decyl chains to the original methyl groups of the resorcinarene rings.[13,14] Then, an initial geometry optimisation of the alkylated resorcinarene structure was achieved with the same program. It was followed by a second optimisation stage of the alkyl chains and H atoms, carried out at the PM7 level of theory with the program Gaussian.[12]

MD simulations were carried out with the software Gromacs2021, at 300 K and 1 bar.[15] The negatively charged ions, ClO_4^- or BAr^{F-}, were initially placed at a distance of about 3.3 nm or larger from the cage surface. The systems were then solvated using a box of chloroform saturated with water. The initial chloroform box, containing 1000 $CHCl_3$ molecules, was retrieved from the VirtualChemistry server.[16] Six water molecules were added at random positions using the Gromacs *insert* tool[15] to reach saturation concentration at 300 K, i.e., a mole fraction of 5.744 10^{-3} at 25°C which corresponds to a concentration of 69 mM of water, as reported in the IUPAC solubility database.[17] Solvation of the system with water and chloroform was carried out with the Gromacs *solvate* tool.[15] It was observed that two chloroform molecules were automatically placed inside the cage, in the presence of the ligand, which is consistent with experiments.[10] No water molecules were inserted, due to their very low occurrence in the solvation box.

The atomic charges of the resorcinarene structure, the $CuTMPAN_3$ complex, the BAR^{F-}, and ClO_4^- ions were obtained from electrostatic maps calculated at the QM B3LYP-631G* level of theory. More precisely, electrostatic potential grids were generated with the Gaussian tool *cubegen* using medium level of coarseness. The atomic charges were then fitted, by a least-square procedure, using the program QFIT[18] which allows to assign a same charge value to atoms of the same type. A modified version of QFIT was used wherein electrostatic forces are fit rather than electrostatic potential values.[19] Fits were achieved by considering grid points located at distances between 1.4 and 2.0 times the van der Waals radius of the atoms, as well as a constraint on the total net charge. These two distance values were selected after the so-called Merz-Singh-Kollman scheme.[20] Charge values are reported in Table S3. The Cu ion charge is largely smaller than the oxidation state (+2). It actually allows to better fit the experimental data by avoiding coordination of water to the metal ion. The van der Waals parameters of the Cu^{2+} ion were taken from the work of Bogetti et al.[21]

Atom type	Net charge	Atom type	Net charge
Methyl_resorcinarene	MSD electrostatic pot = 0.559 (kcal/mol)^2		
1	-0.6016	7	0.0581
2	0.4338	8	0.0780
3	-0.4515	9	0.4906
4	0.1978	10	0.0278
5	0.3821	11	-0.6276
6	-0.33085	12	0.1533
Undecyl_resorcinarene	MSD electrostatic pot = 0.460 (kcal/mol)^2		
1	-0.5811	9	0.2309
2	0.4179	10	0.02985
3	-0.4293	11	-0.1087
4	0.1708	12	0.04198
5	0.3873	13	-0.06385
6	-0.2255	14	0.032405
7	-0.1061	15	-0.08127
8	0.1312	16	0.02424
CuTMPAN$_3$	MSD electrostatic pot = 0.507 (kcal/mol)^2		
1	0.2990	9	0.1990
2	-0.4366	10	0.0288
3	0.1731	11	0.1731
4	0.4240	12	-0.3922
5	-0.13695	13	0.2063
6	0.0822	14	0.04967 (Cu)
7	0.132766	15	-0.5109(N3_outer)
8	-0.2618	16	0.5805 (N3_inner)
ClO$_4^-$	MSD electrostatic pot = 0.100 (kcal/mol)^2		
1	-0.4960 (O)	2	0.9840 (Cl)
BAR^{F-}	MSD electrostatic pot = 0.124 (kcal/mol)^2		
1	0.3232	6	-0.5984 (B)
2	-0.3067	7	-0.1735 (F)
3	0.0726	8	0.1525
4	-0.2842	9	0.1558
5	0.4545		

Table S3. Calculated atomic net charges of resorcinarene, the ligand, and the anions, obtained using the program QFIT[18] and B3LYP-631G*/MK electrostatic potential grids. Final QFIT mean square deviation (MSD) values are reported. Atom types are given in Figure S36.

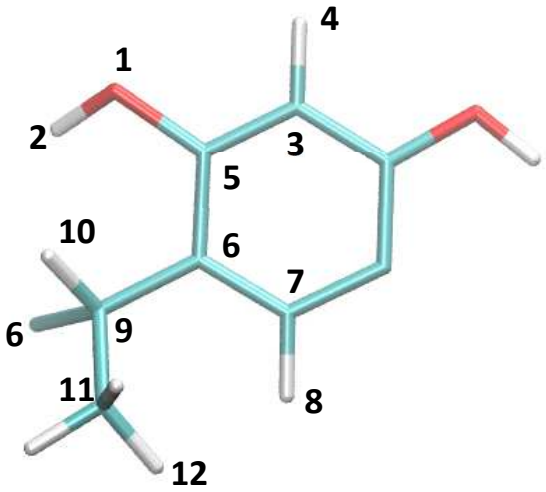

Resorcinarene (R = CH_3)

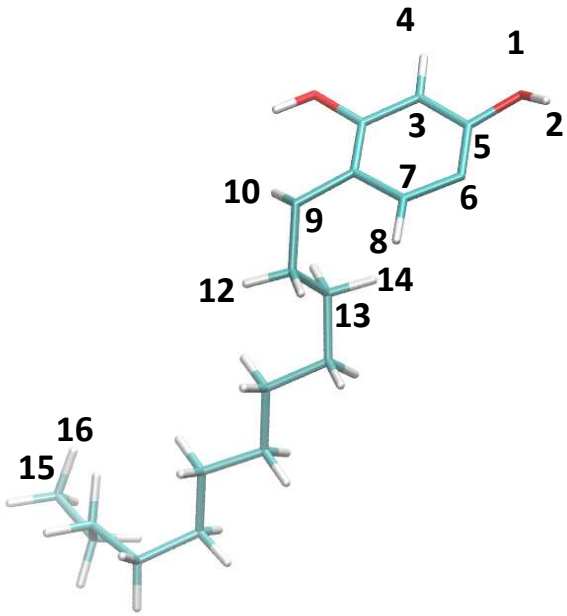

Resorcinarene (R = $C_{11}H_{23}$)

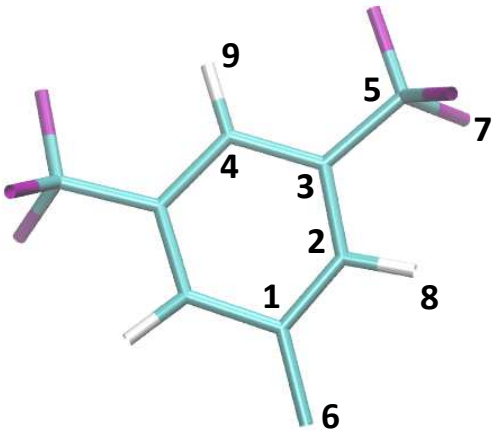

BARF

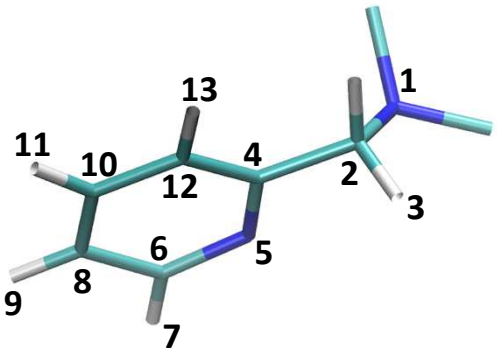

TMPA

Figure S36. Atom types used for charge assignments using QFIT. Only parts of the molecular structures are shown.

The charge values were included in *.mol2* files which were submitted to the Acpype server[22] (with the option *user charges*) to generate coordinates and OPLSAA topology files for resorcinarene (R = CH_3 or $C_{11}H_{23}$), TMPA, ClO_4^-, and BAr^{F-}, suitable for the program Gromacs.

As N_3^- is a linear ion, its topology was built similarly to CO_2, where the ion is described by three atoms bearing the charges and two virtual sites bearing the masses, as described in a Gromacs tutorial.[23]

Water was modeled with either the rigid TIP3P or SPC/E forcefields, which are often used with the OPLSAA FF. The TIP3P water geometry is closer to the experimental one with an angle of 104.5°, while SPC/E (angle = 109.47 °) is known to lead to better diffusion coefficient for liquid water and has been used in previous works.[24,25]

To eliminate large forces, the complete systems were optimised to eliminate large forces using a Steepest Descent procedure with a tolerance of 1.0 kJ mol^{-1} nm^{-1} and an initial step size of 0.05 nm. A maximum number of 5,000 iterations was allowed. The systems were then heated to 50 K through a 10 ps NVT MD, with a time step of 2 fs and LINCS constraints acting on bonds involving H atoms. Each trajectory was followed by two successive 20 ps heating stages, at 150 and 300 K under the same conditions. The equilibration stage was continued for 60 ns in the NPT ensemble, using the thermostat V-rescale and barostat Berendsen algorithms. Finally, the production stage was carried out for 20 ns in the NPT ensemble using the same control algorithms. Snapshots were saved every 2 fs.
During all MD simulations, the van der Waals cut-off distance was set equal to 1 nm with long-range energy and pressure corrections, as required for the OPLSAA forcefield. A Particle Mesh Ewald (PME) Periodic Boundary Conditions (PBC) scheme was applied to calculate the long-range electrostatic interactions with a cut-off of 1 nm as well.
As the CuTMPAN3 ligand is decomposed into three distinct components, coordination bonds are mimicked by distance and angle restraints to avoid too strong a deformation during the MD simulations (Table S4). Such constraints allow to preserve the triangular bipyramidal geometry around the metal ion. Distance and angle restraints were applied between the Cu cation and the four N atoms of the TMPA structure, as well as between the Cu cation and the closest nitrogen atom of the azide component.
A total of eight MD simulations were carried out as listed in Table S5.

[bonds]
Ntop is the central N atom of TMPA

atom1	atom2	type	lower limit (nm)	first upper limit	2nd upper limit	force constant (kJ/mol/nm²)
Ntop	Cu	10	0.2	0.205	0.205	10,000
N2	Cu	10	0.2	0.207	0.210	10,000
N3	Cu	10	0.2	0.207	0.210	10,000
N4	Cu	10	0.2	0.207	0.210	10,000
N_{N3}	Cu	10	0	0.195	0.250	50,000

[angles]
C1, C2, C3 are the carbon atoms of the TMPA aromatic rings, located at para positions of the $N(CH2)_3$ group

atom1	atom2	atom3	type	angle (°)	force constant (kJ/mol/rad²)
C1	C2	C3	1	60	1,000
C2	C3	C1	1	60	1,000
C3	C1	C2	1	60	1,000
Ntop	N_{N3}	Cu	1	0	1,000

Table S4. Intermolecular interaction constraints as implemented in the topology file of the $CuTMPAN_3$ ion.

In addition to the eight conventional MD simulations described in Table S5, four short SMD calculations, which require the application of a pulling force on a selected part of the system, were carried out to confirm the energetics data. To do so, the complexes were incorporated in a large cubic box of at least 9 nm long and were submitted to an equilibration stage of 20.050 ns in the same conditions as applied for the conventional MD simulations. Then, the SMD stage consisted in applying a pulling force to a single resorcinarene centre of mass while restraining the position of the carbon atoms of the aromatic rings bonded to the alkyl-substituted C atoms of the other resorcinarene rings. The SMD pulling stage was carried out for 30,000 iterations, with a time step of 2 fs, a harmonic "umbrella" force constant of 1,000 kJ mol^{-1} nm^{-2}, and a pulling rate of 0.025 nm ps^{-1}. The SMD simulations were applied to the $\mathbf{1}_6^1$- systems which rapidly converge towards an equilibrium state.

MD code	R	Water FF	Final box size (nm)	Total # of H_2O	Total # of $CHCl_3$
$\mathbf{1}_6^1$-PER-T	CH_3	TIP3P	6.16502	22	1743
$\mathbf{1}_6^1$-PER-S	CH_3	SPC/E	6.16855	22	1743
$\mathbf{1}_6^1$-BRF-T	CH_3	TIP3P	6.15597	22	1735
$\mathbf{1}_6^1$-BRF-S	CH_3	SPC/E	6.16580	22	1735
$\mathbf{1}_6^{11}$-PER-T	$C_{11}H_{23}$	TIP3P	8.22098	30	4125
$\mathbf{1}_6^{11}$-PER-S	$C_{11}H_{23}$	SPC/E	8.21911	30	4125
$\mathbf{1}_6^{11}$-BRF-T	$C_{11}H_{23}$	TIP3P	10.12041	50	7760
$\mathbf{1}_6^{11}$-BRF-S	$C_{11}H_{23}$	SPC/E	10.11158	50	7760

Table S5. MD simulation conditions.

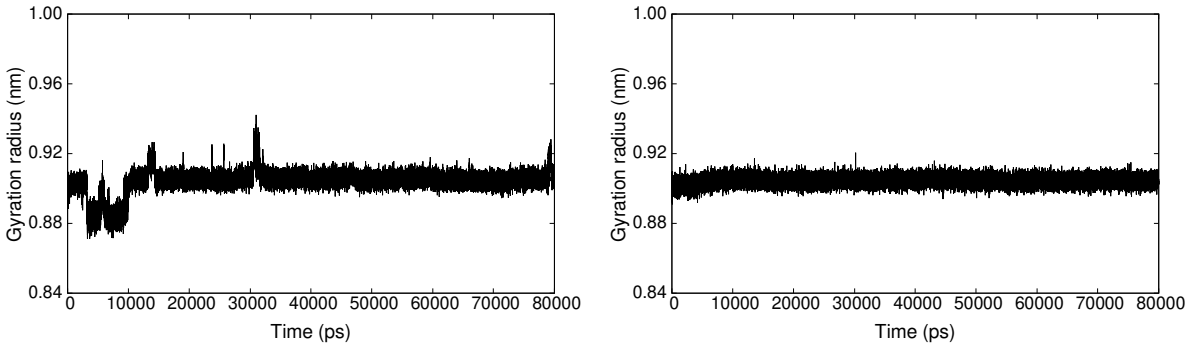

$\mathbf{1}_6^1$-PER
0.905 ± 0.003

$\mathbf{1}_6^1$-BRF
0.904 ± 0.003

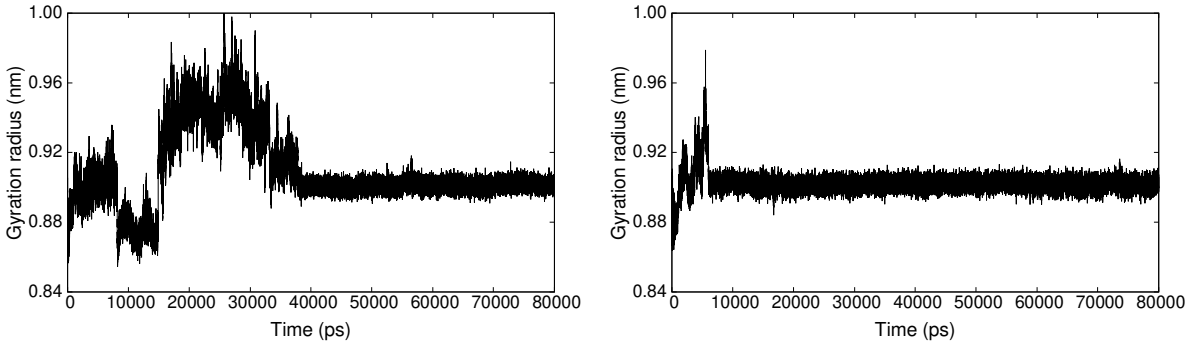

$\mathbf{1}_6^{11}$-PER
0.909 ± 0.002

$\mathbf{1}_6^{11}$-BRF
0.902 ± 0.003

Figure S37. Gyration radius profiles of the resorcinarene cage calculated from the MD simulations (equilibration and production stages). Water is described using the TIP3P FF. Average and standard deviation values (nm) are calculated over the last 20 ns of the simulations.

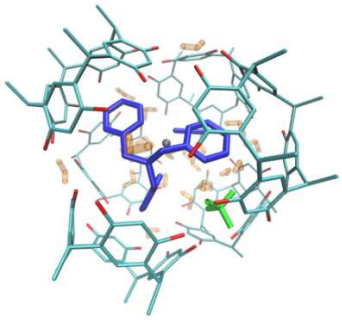

$\mathbf{1}_6^1$-PER-T

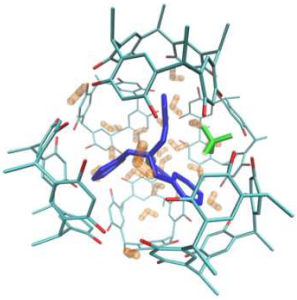

$\mathbf{1}_6^1$-PER-S

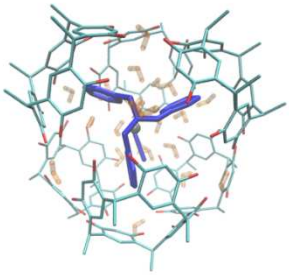

$\mathbf{1}_6^1$-BRF-T

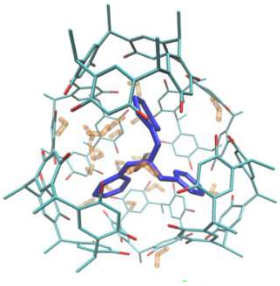

$\mathbf{1}_6^1$-BRF-S

$\mathbf{1}_6^{11}$-PER-T

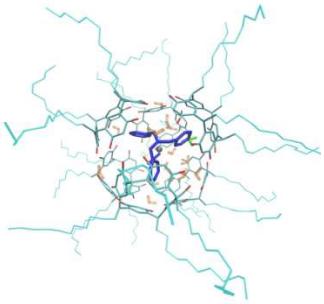

$\mathbf{1}_6^{11}$-PER-S

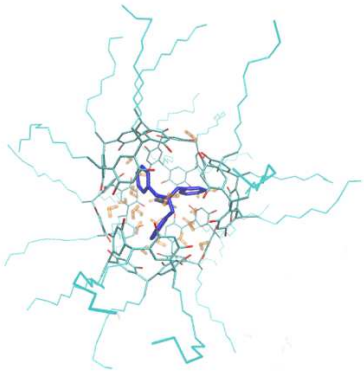

$\mathbf{1}_6^{11}$-BRF-T

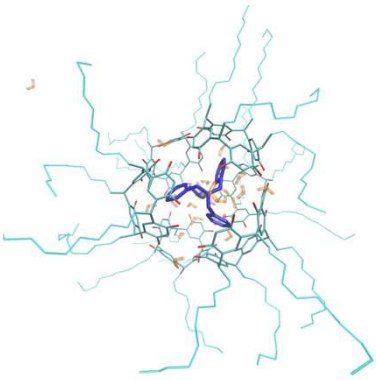

$\mathbf{1}_6^{11}$-BRF-S

Figure S38. Last frame of the MD simulations (perspective views). Ligand = dark blue, Cu ion = gray sphere, water = orange, anion = green, resorcinarene = cyan (alkyl chains are shown with thin lines). H atoms are not shown for clarity.

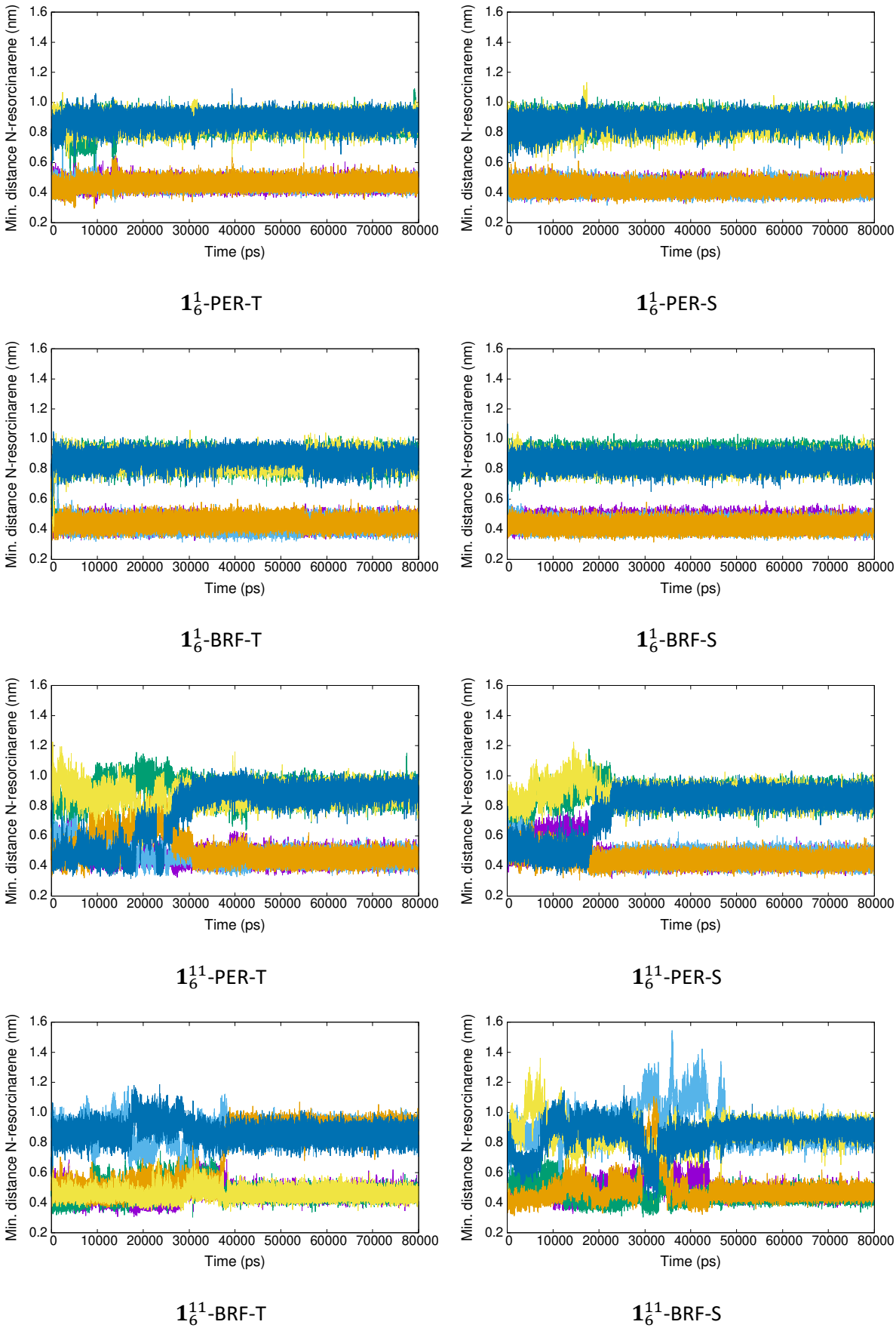

Figure S39. The six N_{top}-resorcinarene minimal distance profiles obtained from the MD simulations.

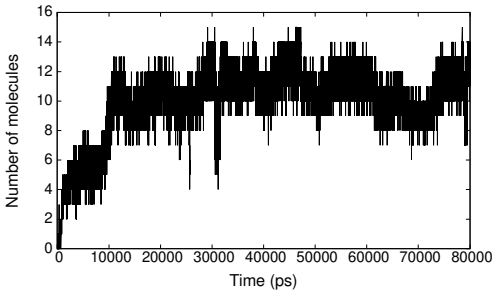

$\mathbf{1}_6^1$-PER-T

10.6 ± 1.3

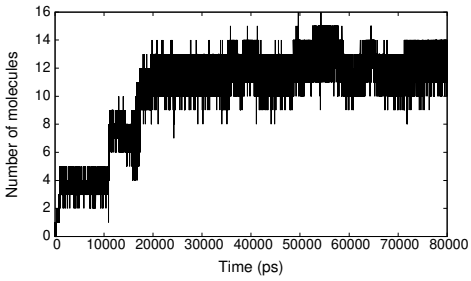

$\mathbf{1}_6^1$-PER-S

12.2 ± 1.0

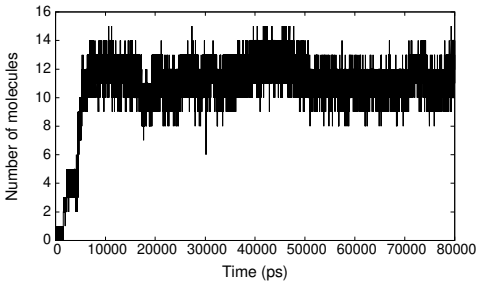

$\mathbf{1}_6^1$-BRF-T

11.2 ± 0.9

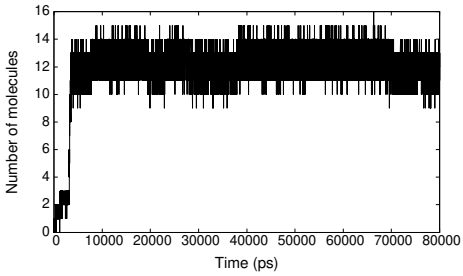

$\mathbf{1}_6^1$-BRF-S

12.5 ± 0.9

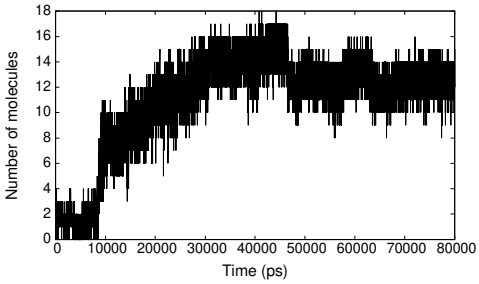

$\mathbf{1}_6^{11}$-PER-T

12.7 ± 1.1

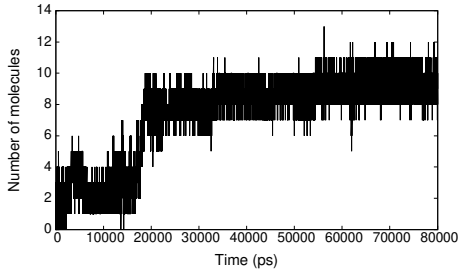

$\mathbf{1}_6^{11}$-PER-S

9.6 ± 0.7

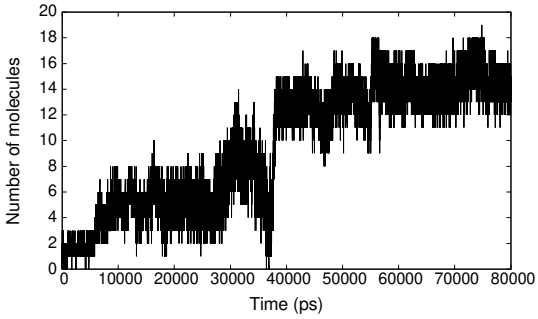

$\mathbf{1}_6^{11}$-BRF-T

14.4 ± 1.2

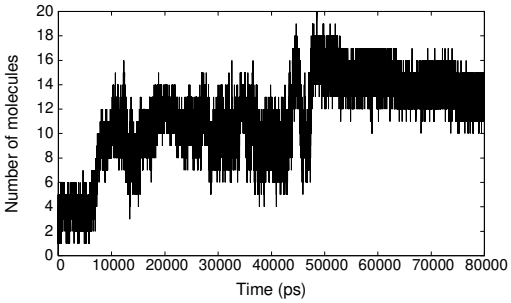

$\mathbf{1}_6^{11}$-BRF-S

13.7 ± 1.0

Figure S40. Number of water molecules located below 0.6 nm from the centre of mass of the resorcinarene cage, obtained from the MD simulations (equilibration and production stages). Averages and standard deviation values are calculated over the last 20 ns of the trajectories.

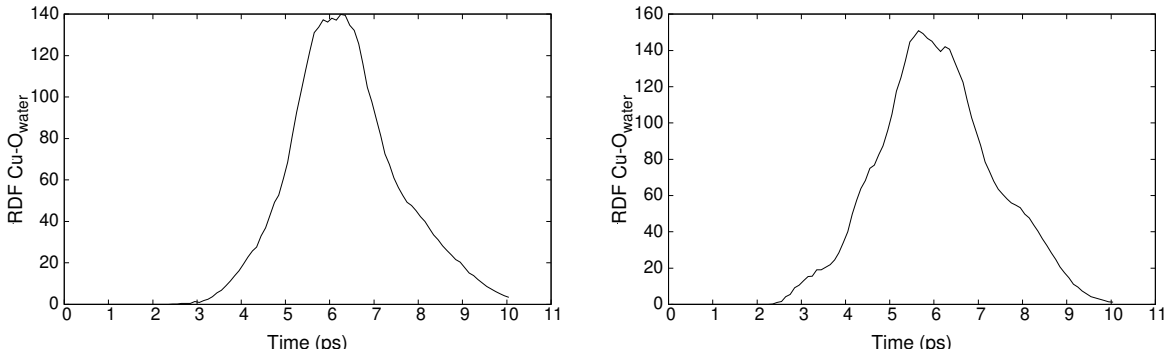

$\mathbf{1}_6^1$-PER-T

$\mathbf{1}_6^1$-PER-S

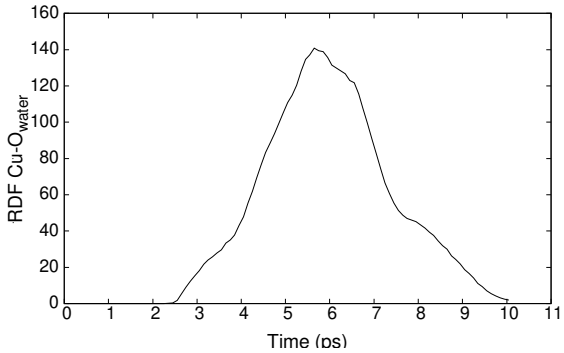

$\mathbf{1}_6^1$-BRF-T

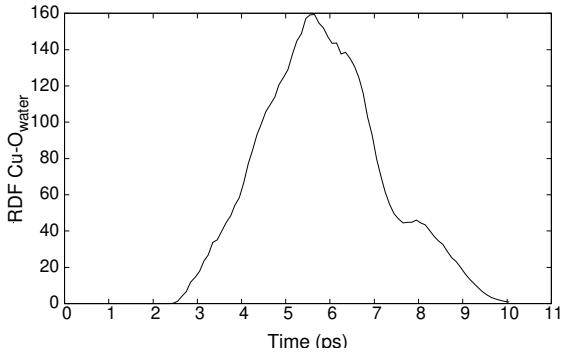

$\mathbf{1}_6^1$-BRF-S

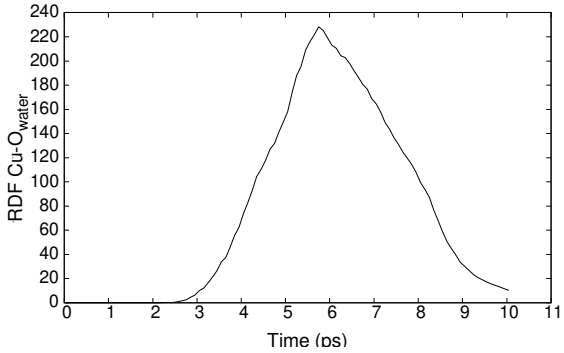

$\mathbf{1}_6^{11}$-PER-T

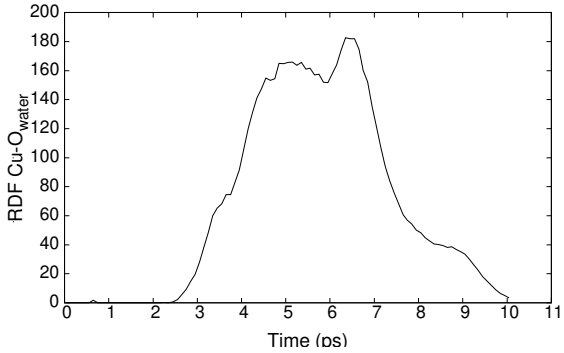

$\mathbf{1}_6^{11}$-PER-S

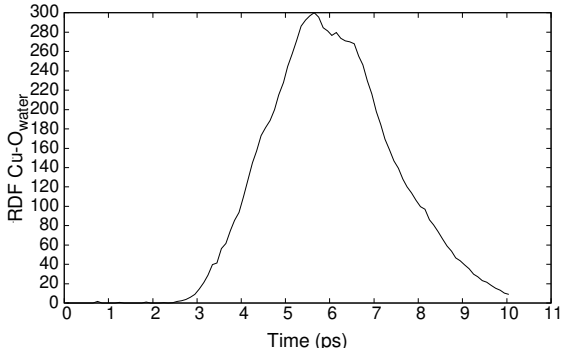

$\mathbf{1}_6^{11}$-BRF-T

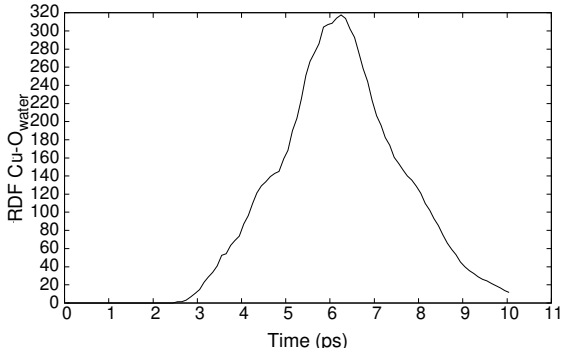

$\mathbf{1}_6^{11}$-BRF-S

Figure S41. Radial distribution function g(Cu-O_{water}) calculated over the last 20 ns of the MD simulations using the program VMD.[26]

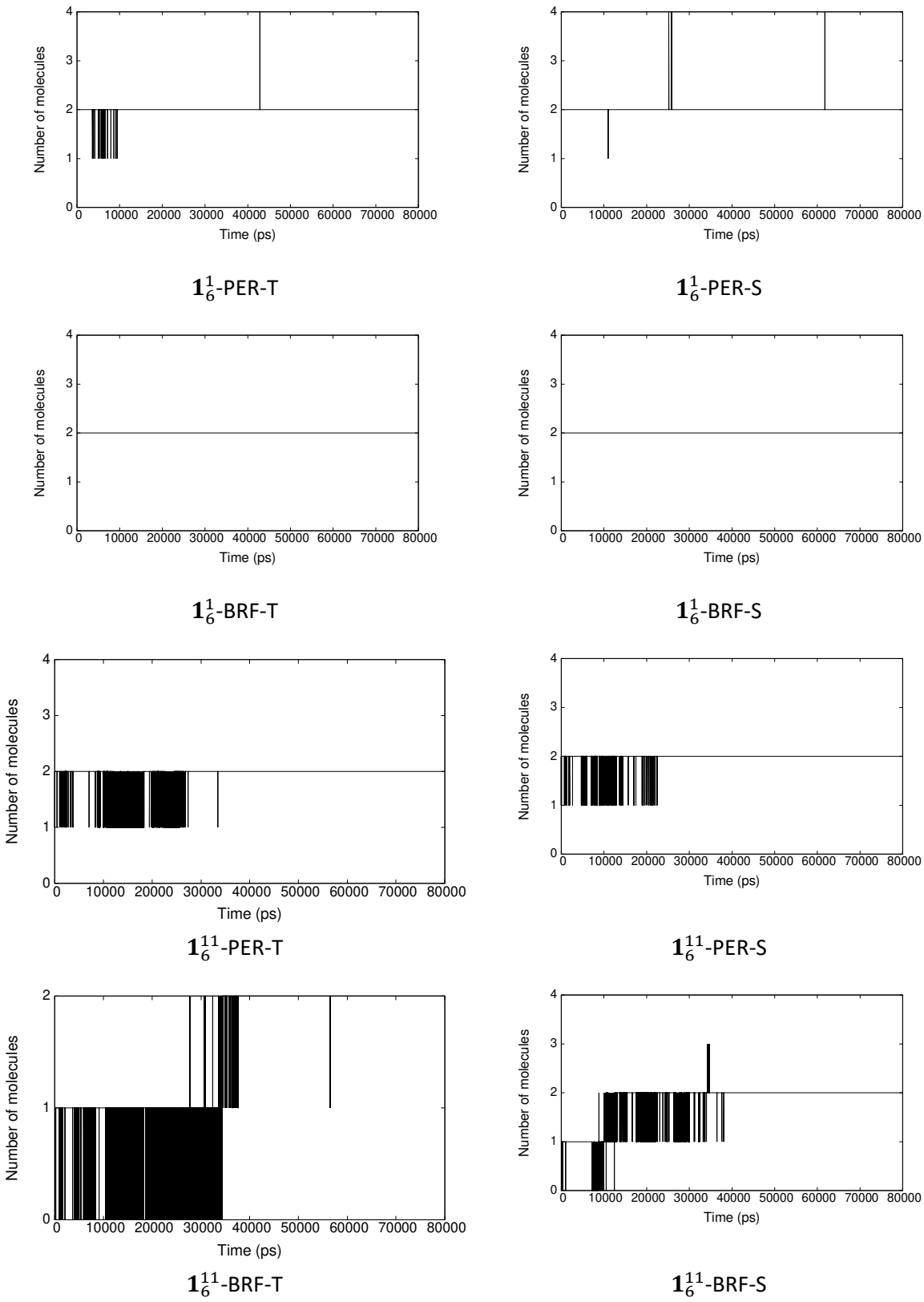

Figure S42. Number of chloroform molecules located below 0.6 nm from the resorcinarene cage centre-of-mass calculated from the MD simulations.

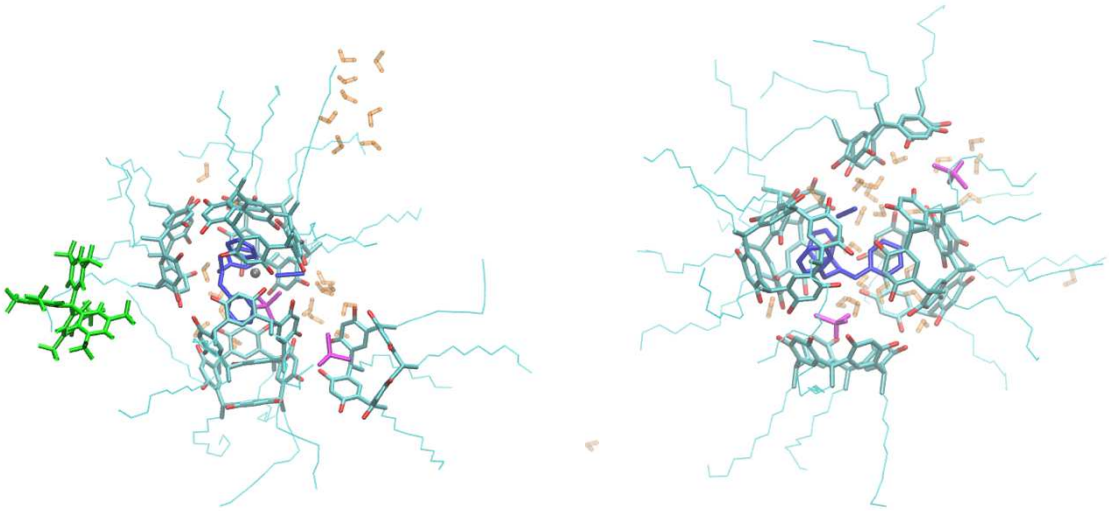

Figure S43. Snapshots of the MD simulation of the (left) $\mathbf{1}_6^{11}$-BRF-S system at t = 6,498 ps and (right) $\mathbf{1}_6^{11}$-BRF-T system at t = 33,468 ps. Ligand = blue, Cu ion = gray sphere, water = orange, BARF = green, resorcinarene = cyan (alkyl chains are shown with thin lines), chloroform = magenta. H atoms are not shown for clarity.

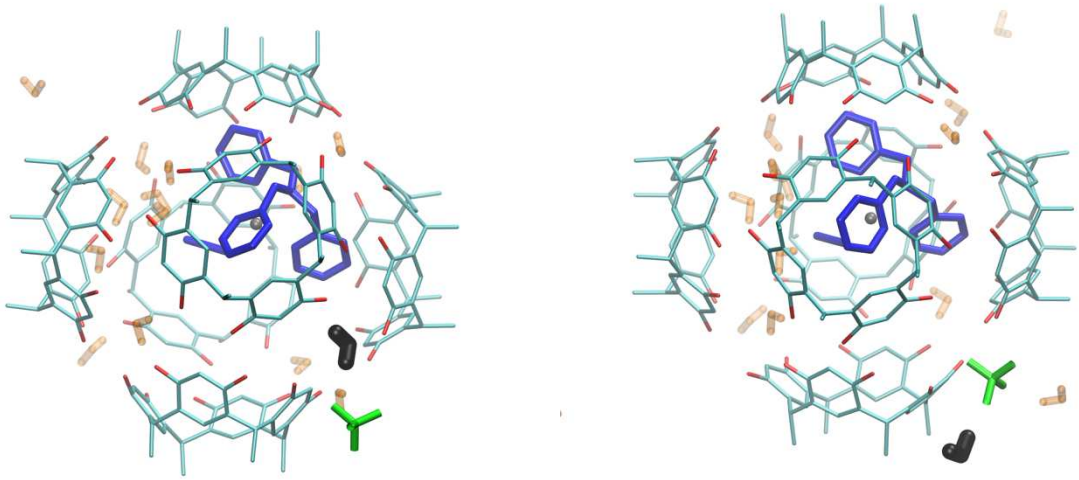

Figure S44. Snapshots of the MD simulation of the $\mathbf{1}_6^{1}$-PER-T system at t = 1,758 ps (left) and t = 1,916 ps (right). Ligand = blue, Cu ion = gray sphere, water = orange, PER = green, resorcinarene = cyan. The replaced structuring water molecule is displayed with thick black sticks. H atoms are not shown for clarity.

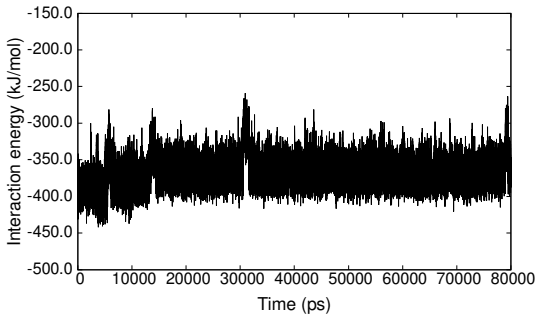

$\mathbf{1}_6^1$-PER-T
-367.9 $\pm$ 17.8

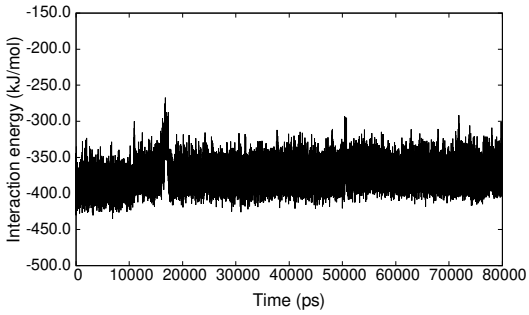

$\mathbf{1}_6^1$-PER-S
-372.6 $\pm$ 15.6

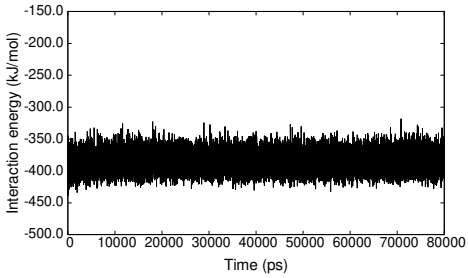

$\mathbf{1}_6^1$-BRF-T
-385.9 $\pm$ 13.7

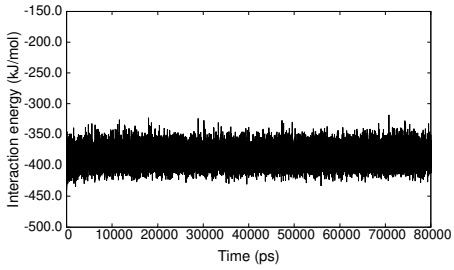

$\mathbf{1}_6^1$-BRF-S
-385.6 $\pm$ 13.3

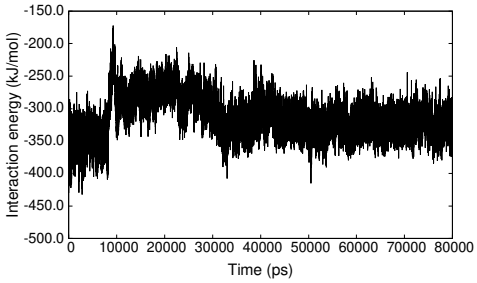

$\mathbf{1}_6^{11}$-PER-T
-324.6 $\pm$ 18.2

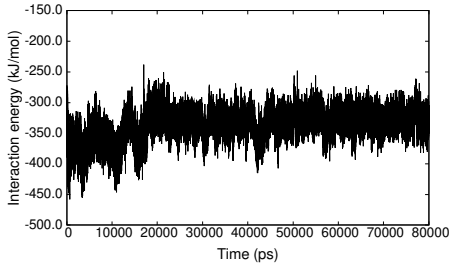

$\mathbf{1}_6^{11}$-PER-S
-328.8 $\pm$ 15.9

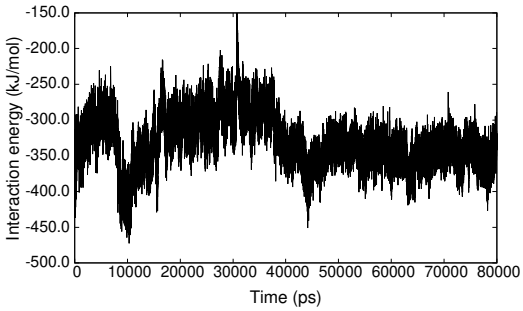

$\mathbf{1}_6^{11}$-BRF-T
-349.9 $\pm$ 19.2

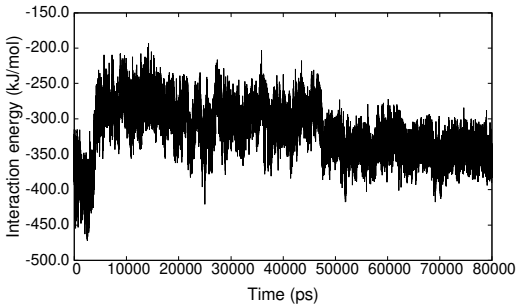

$\mathbf{1}_6^{11}$-BRF-S
-344.3 $\pm$ 17.6

Figure S45. Sum over all resorcinarene-resorcinarene interaction energy contributions obtained from each MD simulations. Averages and standard deviations (kJ/mol) are calculated over the last 20 ns of the trajectories.

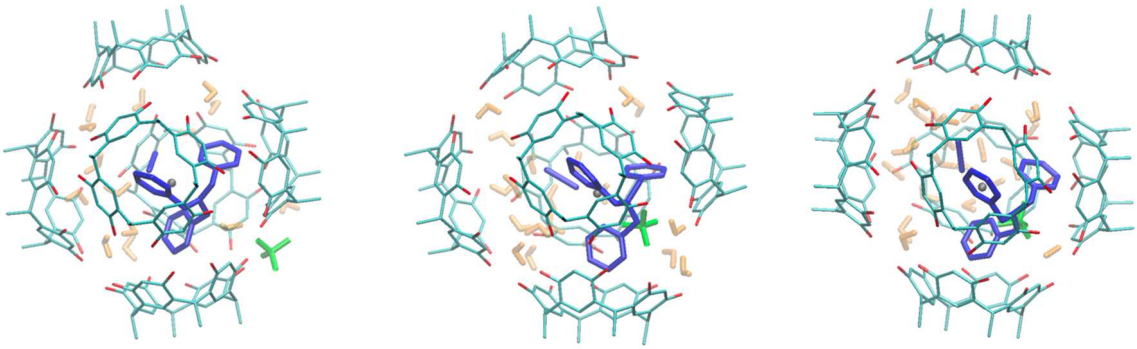

Figure S46. Snapshots of the MD simulation of the $\mathbf{1}_6^1$-PER-T system at t = 5,714 ps (left), at t = 13,788 ps (middle), and t = 16,768 ps (right). Ligand = blue, Cu ion = gray sphere, water = orange, PER = green, resorcinarene = cyan. H atoms are not shown for clarity.

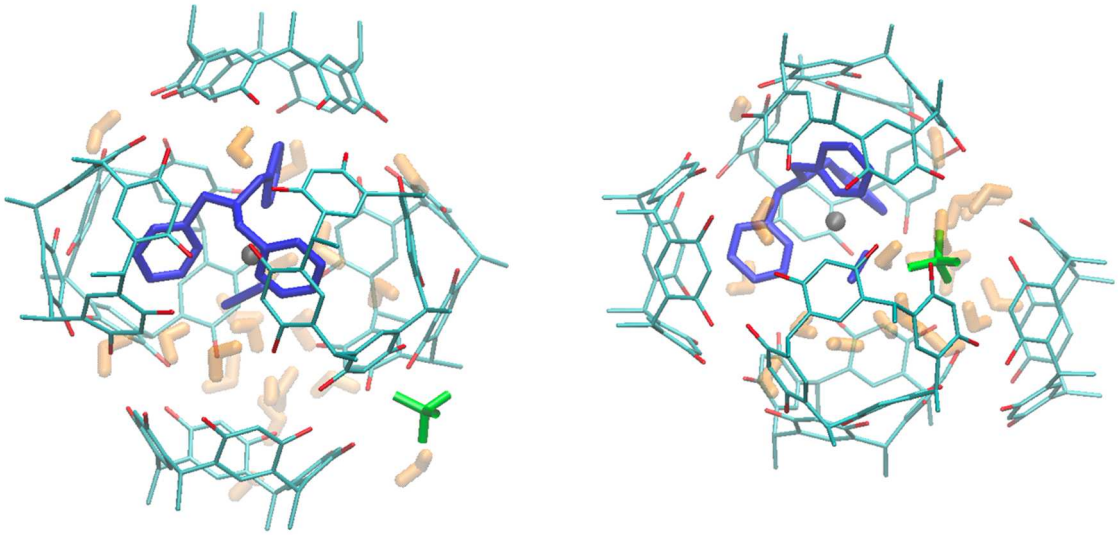

Figure S47. Snapshots of the MD simulation of the $\mathbf{1}_6^1$-PER-S system at t = 10,920 ps (left) and t = 16,768 ps (right). Ligand = blue, Cu ion = gray sphere, water = orange, PER = green, resorcinarene = cyan. H atoms are not shown for clarity.

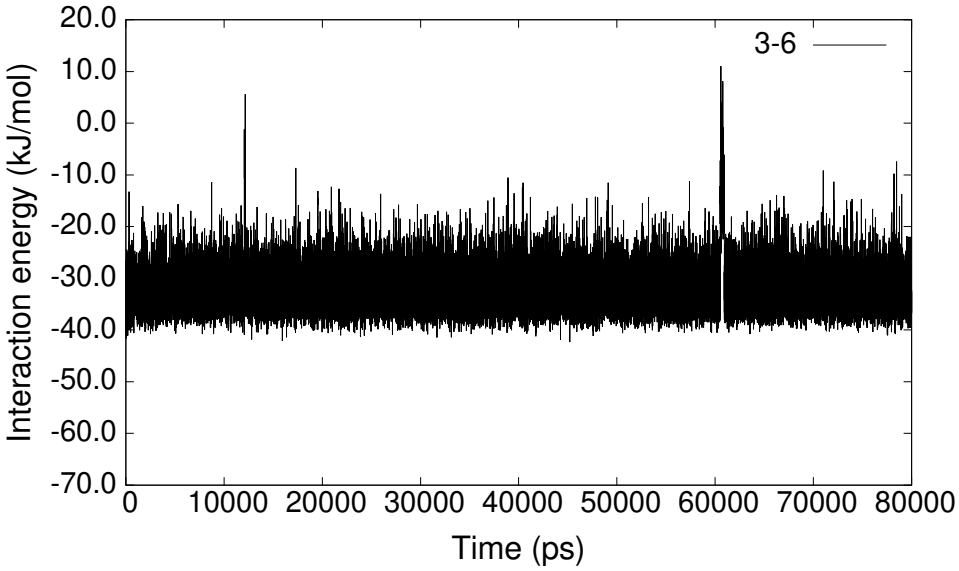

Figure S48. Single resorcinarene-resorcinarene interaction energy profiles obtained from the MD simulation of system $\mathbf{1}_6^1$-BRF-S.

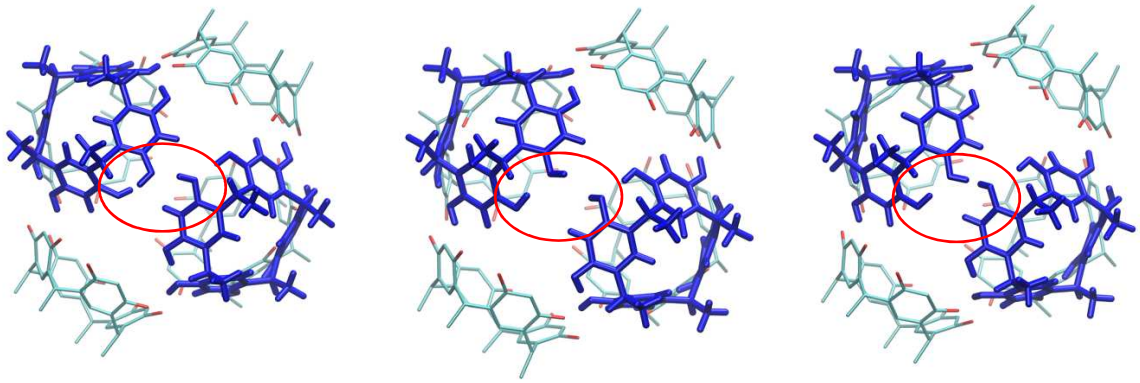

Figure S49. Snapshots of the MD simulation of the $\mathbf{1}_6^1$-BRF-S system at t = 60,526 ps (left), t = 60,684 ps (centre), and t = 60,700 ps (right). Involved resorcinarene rings are displayed with dark blue sticks.

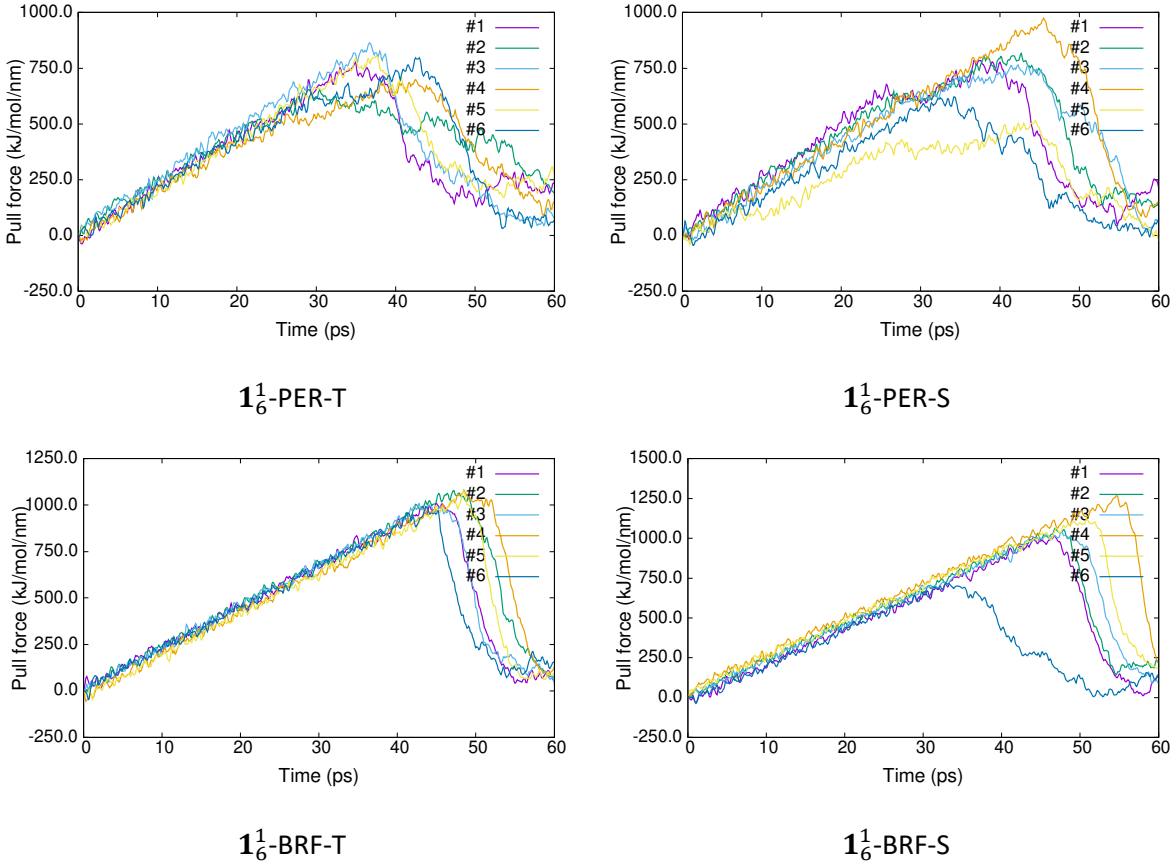

$\mathbf{1}_6^1$-PER-T $\mathbf{1}_6^1$-PER-S

$\mathbf{1}_6^1$-BRF-T $\mathbf{1}_6^1$-BRF-S

Figure S50. Profiles of the pull force felt by each of the six resorcinarene rings during the 60 ps long pulling stage of the SMD simulations. The force values involve all elements of the systems.

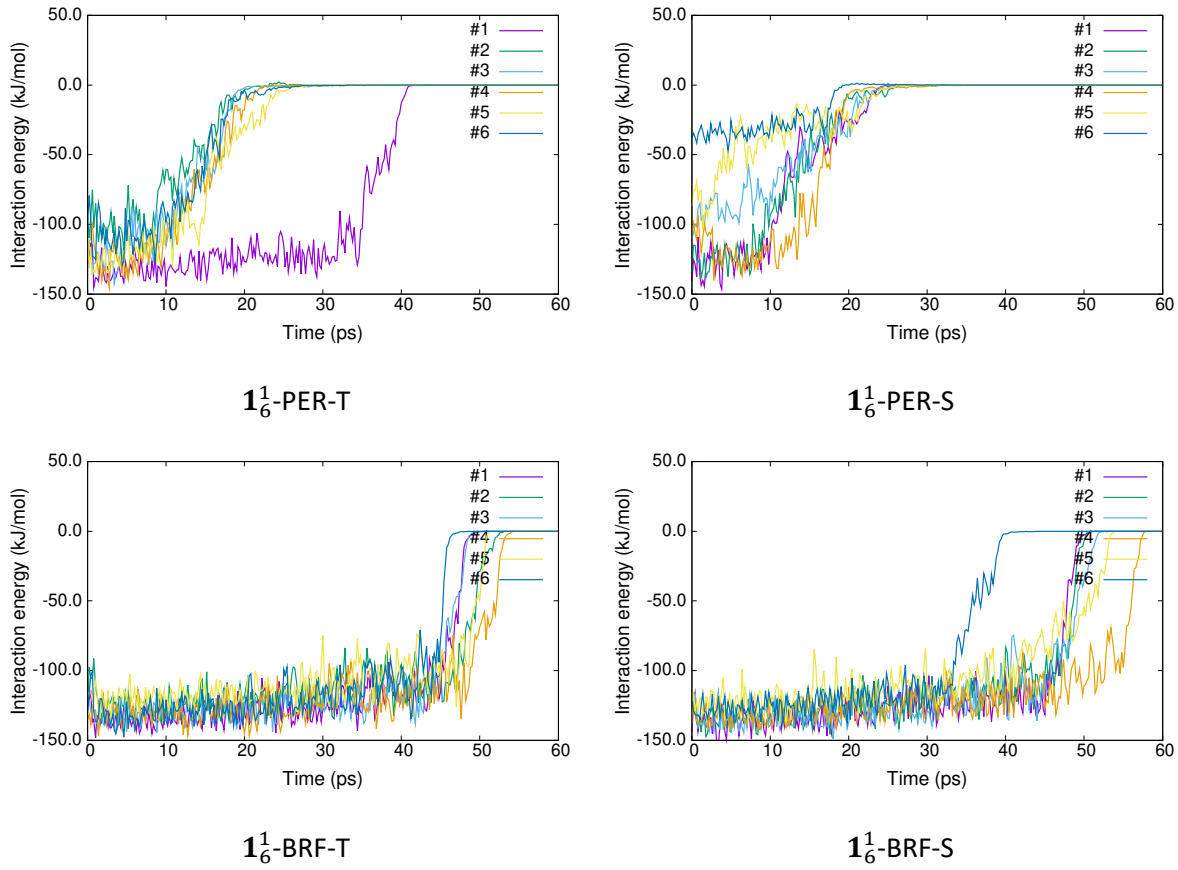

$\mathbf{1}_6^1$-PER-T $\mathbf{1}_6^1$-PER-S

$\mathbf{1}_6^1$-BRF-T $\mathbf{1}_6^1$-BRF-S

Figure S51. Profiles of each of the six resorcinarene interaction energy during the 60 ps long pulling stage of the SMD simulations. The energy values involve the resorcinarene elements only.

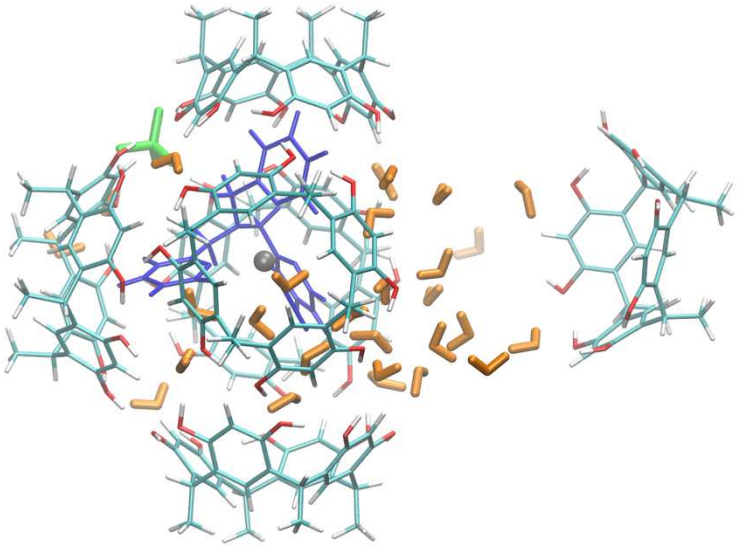

Figure S52. Snapshot of the SMD simulation of the $\mathbf{1}_6^1$-PER-T system at t = 41.6 ps of the pulling stage of resorcinarene #1. Ligand = blue, Cu ion = gray sphere, water = orange, PER = green, resorcinarene = cyan.

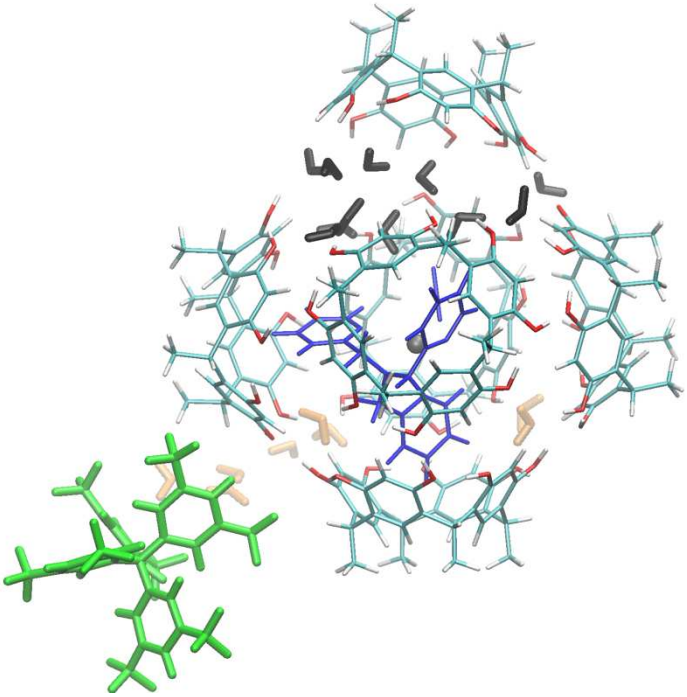

Figure S53. Snapshot of the SMD simulation of the $\mathbf{1}_6^1$-BRF-S system at t = 36.4 ps of the pulling stage of resorcinarene #6. Ligand = blue, Cu ion = gray sphere, water = orange, BARF = green, resorcinarene = cyan. The water molecules close to resorcinarene #6 is displayed using thick black sticks.

7- Reactivity

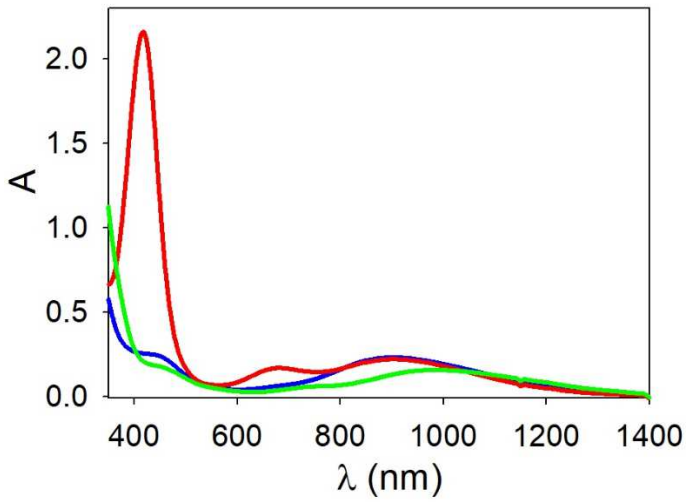

Figure S54. UV-vis spectra of a 1:1 mixture of **1_6** and **[TMPACu(H_2O)](ClO_4)$_2$** before (blue) and after the addition of 1 equiv. of (NBu_4)N_3 (red) and (NBu_4)Cl (green) ($CHCl_3$, 298 K, 1 mM).

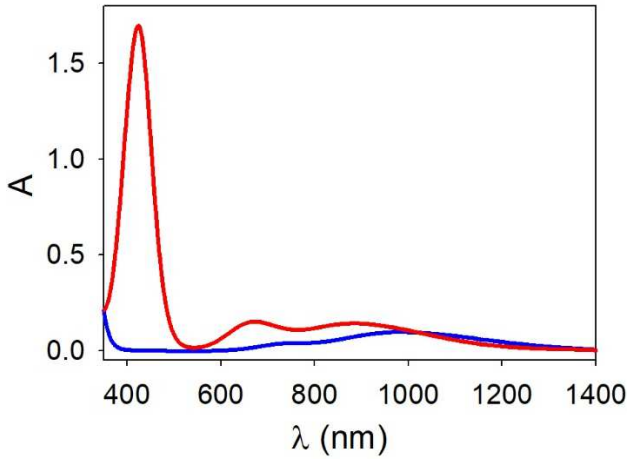

Figure S55. UV-vis spectra of **[TMPACuCl](BAr^F)** before (blue) and after (red) the addition of 1 equiv. of (NBu_4)N_3 ($CHCl_3$, 298 K, 0.5 mM).

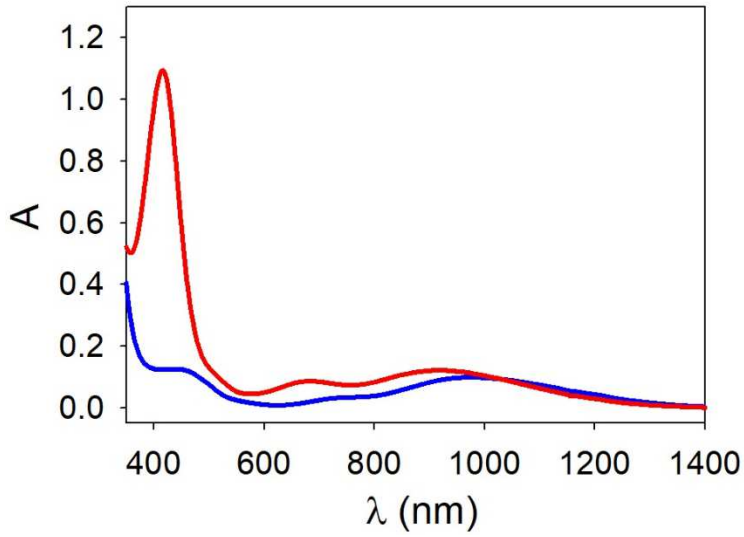

Figure S56. UV-vis spectra of a 1:1 mixture of $\mathbf{1_6}$ and **[TMPACuCl](BAr^F)** before (blue) and after (red) the addition of 1 equiv. of $(NBu_4)N_3$ ($CHCl_3$, 298 K, 0.5 mM).

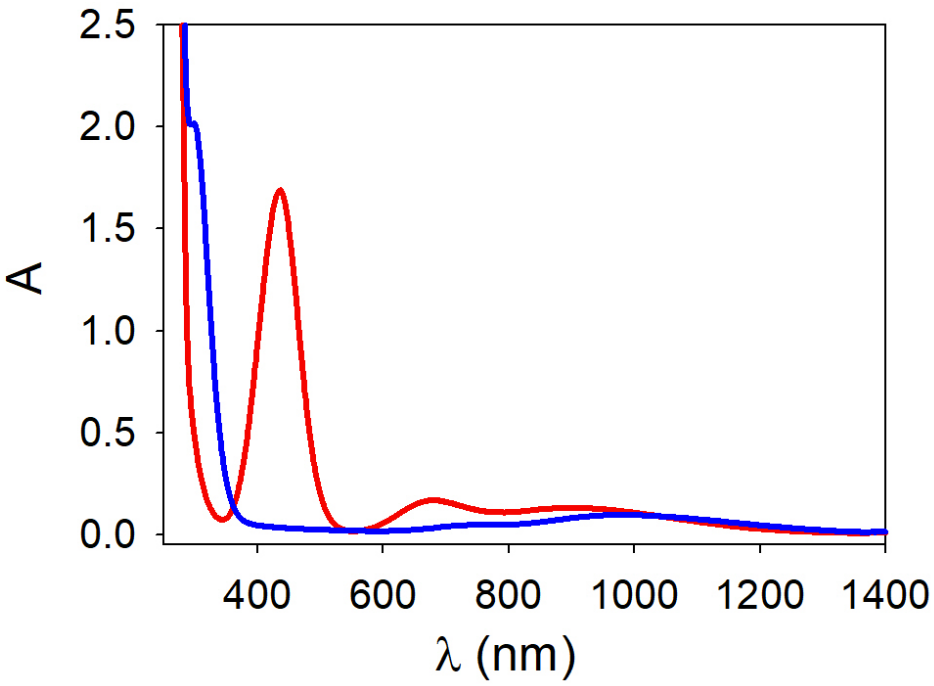

Figure S57. UV-vis spectra of **[TMPACuN$_3$](BAr^F)** before (red) and after (blue) exposition to day light during 2h ($CHCl_3$, 298 K, 0.6 mM).

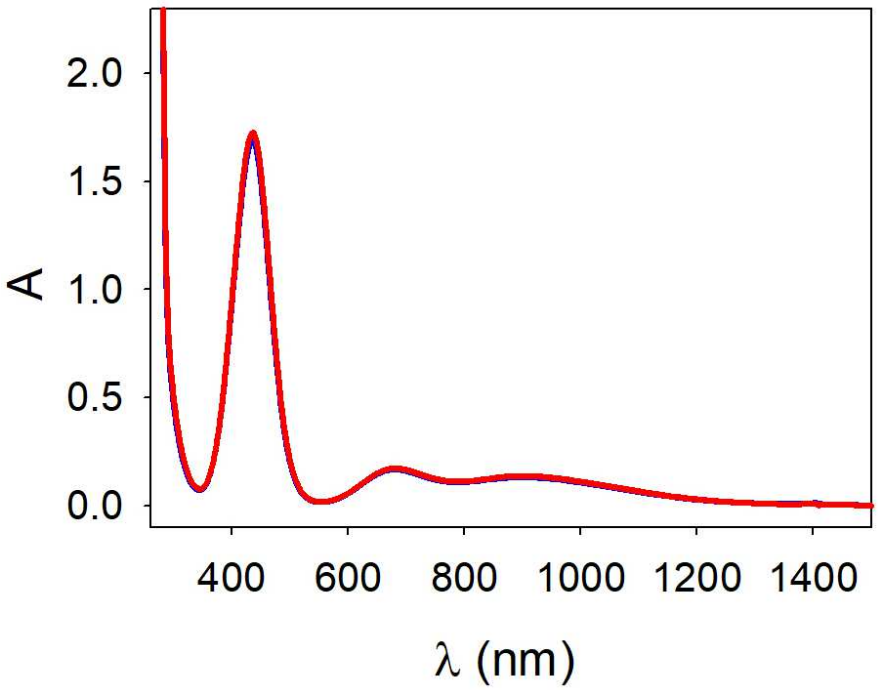

Figure S58. UV-vis spectra of **[TMPACuN$_3$](BAr^F)** before (red) and after (blue) 2h in the dark ($CHCl_3$, 298 K, 0.6 mM).

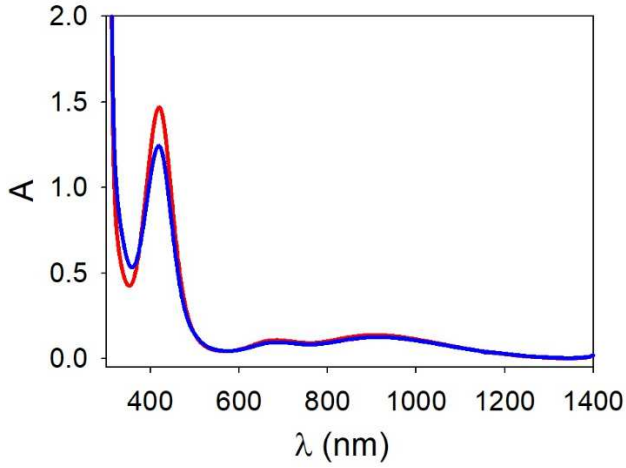

Figure S59. UV-vis spectra of a 1:1 mixture of **1$_6$** and **[TMPACuN$_3$](BAr^F)** before (red) and after (blue) exposition to day light during 2h ($CHCl_3$, 298 K, 0.7 mM).

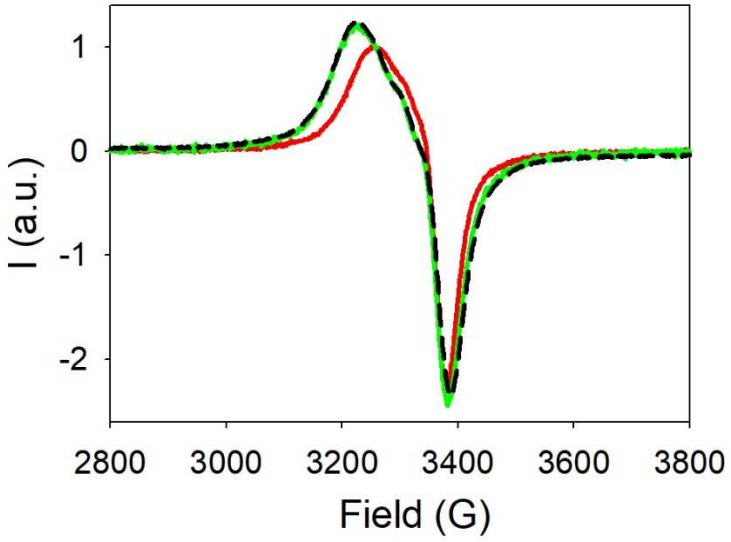

Figure S60. Normalised EPR spectra of **[TMPACuN$_3$](BAr^F)** before (red) and after (green) irradiation at 420 nm during 15 min and **[TMPACuCl](BAr^F)** (black dashed line) ($CHCl_3$, 298 K).

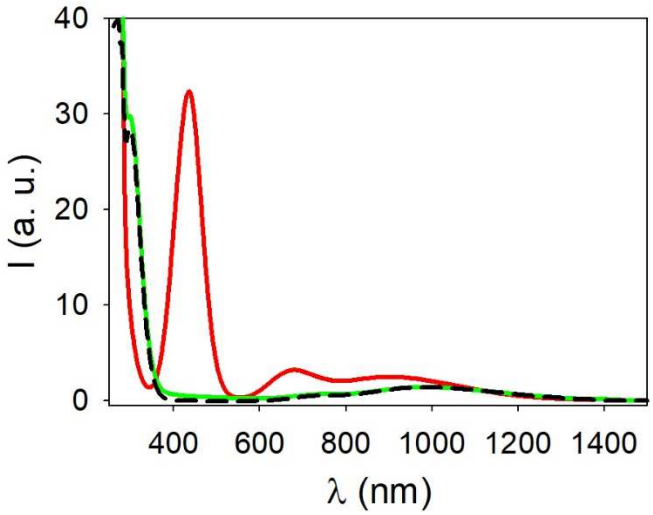

Figure S61. Normalised UV-vis spectra of **[TMPACuN$_3$](BAr^F)** before (red) and after (green) irradiation at 420 nm during 15 min and **[TMPACuCl](BAr^F)** (black dashed line) ($CHCl_3$, 298 K).

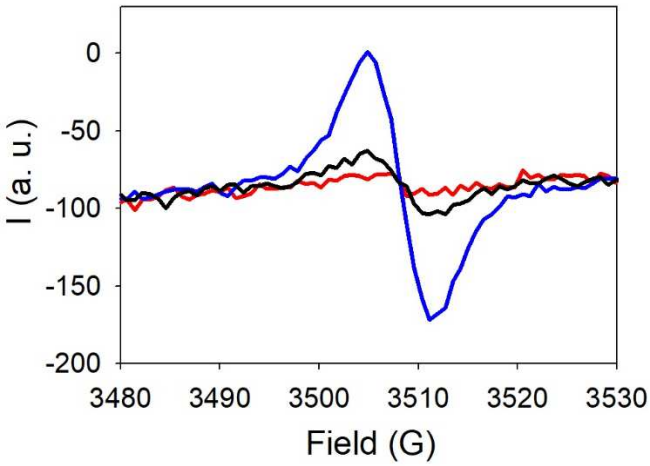

Figure S62. EPR spectra of **[TMPACuN$_3$@1$_6$](BAr^F)** before (red), during irradiation at 420 nm for 15 min (blue) and 15 min after the light was turned off (black) ($CHCl_3$, 298 K, 2.7 mM).

8- References

1 S. Stoll and A. Schweiger, *J. Magn. Reson*. 2006, **178**, 42-55.

2 J. Hartikainen, J. Ruokolainen, K. Rissanen and O. Ikkala, *Synthetic Metals*, 2001, **121**, 1275-1276.

3 T. D. Hamilton, G. S. Papaefstathiou, T. Friščić, D.-K. Bučar and L. R. MacGillivray, *J. Am. Chem. Soc*., 2008, **130**, 14366-14367.

4 L. M. Tunstad, J. A. Tucker, E. Dalcanale, J. Weiser, J. A. Bryant, J. C. Sherman, R. C. Helgeson, C. B. Knobler and D. J. Cram, *J. Org. Chem*., 1989, **54**, 1305-1312.

5 Z. Tyeklár, R. R. Jacobson, N. Wei, N. N. Murthy, J. Zubieta and K. D. Karlin, *J. Am. Chem. Soc*., 1993, **115**, 2677-2689.

6 D.M. Corsi, N. N. Murthy, V. G. Young and K. D. Karlin, *Inorg. Chem*., 1999, **38**, 848-858.

7 R. R. Jacobson, Z. Tyeklár, K. D. Karlin and J. Zubieta, *Inorg. Chem*., 1991, **30**, 2035-2040.

8 S. Hematian, M. A. Siegler and K. D. Karlin, *J Am Chem Soc*., 2012, **134**, 18912-18915.

9 A. Wada, Y. Honda, S. Yamaguchi, S. Nagatomo, T. Kitagawa, K. Jitsukawa and H. Masuda, *Inorg. Chem*., 2004, **43**, 5725-5735.

10 T. Zhang, L. Le Corre, O. Reinaud and B. Colasson, *Chem. Eur. J*., 2021, **27**, 434-443.

11 L. Carreras, L. Rovira, M. Vaquero, I. Mon, E. Martin, J. Benet-Buchholza and A. Vidal-Ferran, *RSC Adv*., 2017, **7**, 32833-32841.

12 Gaussian 16, Revision C.01, M. J. Frisch, G. W. Trucks, H. B. Schlegel, G. E. Scuseria, M. A. Robb, J. R. Cheeseman, G. Scalmani, V. Barone, G. A. Petersson, H. Nakatsuji, X. Li, M. Caricato, A. V. Marenich, J. Bloino, B. G. Janesko, R. Gomperts, B. Mennucci, H. P. Hratchian, J. V. Ortiz, A. F. Izmaylov, J. L. Sonnenberg, D. Williams-Young, F. Ding, F. Lipparini, F. Egidi, J. Goings, B. Peng, A. Petrone, T. Henderson, D. Ranasinghe, V. G. Zakrzewski, J. Gao, N. Rega, G. Zheng, W. Liang, M. Hada, M. Ehara, K. Toyota, R. Fukuda, J. Hasegawa, M. Ishida, T. Nakajima, Y. Honda, O. Kitao, H. Nakai, T. Vreven, K. Throssell, J. A. Montgomery, Jr., J. E. Peralta, F. Ogliaro, M. J. Bearpark, J. J. Heyd, E. N. Brothers, K. N. Kudin, V. N. Staroverov, T. A. Keith, R. Kobayashi, J. Normand, K. Raghavachari, A. P. Rendell, J. C. Burant, S. S. Iyengar, J. Tomasi, M. Cossi, J. M. Millam, M. Klene, C. Adamo, R. Cammi, J. W. Ochterski, R. L. Martin, K. Morokuma, O. Farkas, J. B. Foresman, and D. J. Fox, Gaussian, Inc., Wallingford CT, 2016.

13 M. D. Hanwell, D. E. Curtis, D. C. Lonie, T. Vandermeersch, E. Zurek and G. R. Hutchison, *J. Cheminformatics*, 2012, **4**, 17.

14 M. D. Hanwell, D. E. Curtis, D. C. Lonie, T. Vandermeersch, E. Zurek and G. R. Hutchison, "Avogadro: an open-source molecular builder and visualization tool. Version 1.2.0" http://avogadro.cc/, last accessed 18 July 2024.

15 M. J. Abraham, T. Murtola, R. Schulz, S. Páll, J. C. Smith, B. Hess and E. Lindahl, *SoftwareX*, 2015, **1–2**, 19-25.

16 "Classical models", https://virtualchemistry.org/ff.php, last accessed 1 July 2024.

17 IUPAC-NIST solubility database, NIST Standard Reference Database 106, "Solubility System: Trichloromethane (chloroform) with Water", https://srdata.nist.gov/solubility/sol_detail.aspx?goBack=Y&sysID=60_154, last accessed 5 March 2024.

18 O. Borodin and G. D. Smith, "Force field fitting toolkit", The university of Utah, http://www.eng.utah.edu/~gdsmith/fff.html, last accessed 26 August 2009

19 L. Leherte, *Mol. Simul*., 2016, **42**, 289-304.

20 U. C. Singh and P. A. Kollman, *J. Comput. Chem*. 1984, **5**, 129-145.

21 X. Bogetti, S. Ghosh, A. G. Jarvi, J. Wang and S. Saxena, *J. Phys. Chem. B*, 2020, **124**, 2788-2797.

22 a) A. W. Sousa da Silva and W. F. Vranken, *BMC Research Notes* 2012, **5**, 367; b) L. P. Kagami, A. Wilter, A. Díaz and W. F. Vranken, *Bioinformatics*, 2023, **39**, btad350.

23 "GROMACS Tutorial", http://www.mdtutorials.com/gmx/vsites/02_topology.html, last accessed 5 March 2024.

24 A. Katiyar, J. C. Freire Sovierzoski, P. B. Calio, A. A. Vartia and W. H. Thompson, *Chem. Commun.*, 2019, **55**, 6591-6594.

25 D. A. Poole III, S. Mathew and J. N. H. Reek, *J. Am. Chem. Soc.*, 2021, **143**, 16419-16427.

26 W. Humphrey, A. Dalke and K. Schulten, *J. Molec. Graphics*, 1996, **14**, 33-38.